Robust, Bistable, BMP Dependent Patterning of the Drosophila Blastoderm Embryo: Supporting Online Material(SOM)

David Umulis[1], Mihaela Serpe[2,3], Michael B. O'Connor[2,3],

Hans G. Othmer[4]

[1]Department of Chemical Engineering and Materials Science

[2]Department of Genetics, Cell Biology and Development

[3]Howard Hughes Medical Institute

[4]School of Mathematics and Digital Technology Center

University of Minnesota, Minneapolis, MN 55455

July 7, 2006

Contents

List of Figures

List of Tables

1 Extracellular patterning model

The full model for dorsal surface patterning of the *Drosophila* blastoderm embryo is composed of three modules or sub-models that, when combined, lead to the sharp, contracting, robust pattern characteristic of this pathway.

1.1 Model assumptions

1. A deterministic description is used for all processes

2. Production of BMP, Sog, and Tsg is continuous

3. The total number of receptors on the surface remains constant

4. Intracellular reactions (Dimerization, signaling, etc.) are rapid and assumed to be at quasi-equilibrium

5. All non-surface-associated species diffuse

6. Initial amount of unbound receptor is $[R_{tot}]$ and Tld is [Tol]

7. Initial amounts of all other species is zero
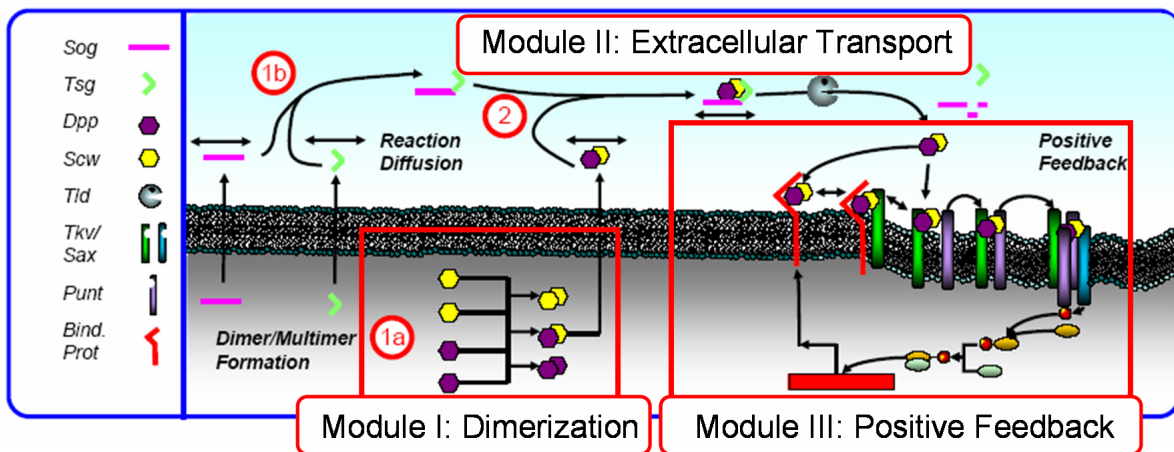
Figure 6: Modules for dorsal surface patterning model with positive feedback of an SBP .

2   Module I: Heterodimer formation

The first module, given in equations 1-3 corresponds to a simplified version of general heterodimer formation of BMPs before secretion into the perivitelline (PV) space [1].

$$\frac{\partial [D]}{\partial t} = \phi_D(x) - K_1[D][W] - K_2[D]^2 \tag{1}$$

$$\frac{\partial [W]}{\partial t} = \phi_W(x) - K_1[D][W] - K_3[W]^2 \tag{2}$$

$$\frac{\partial [DW_{in}]}{\partial t} = K_1[D][W] - \gamma_1[DW_{in}] \tag{3}$$

Here, Dpp (D) and Scw (W) bind to form Dpp/Scw (DWin) which is secreted into the PV space. ϕ_D, and ϕ_W are the production rates of Dpp and Scw respectively, and K_1, K_2, and K_3 are the hetero- and homodimer formation rates. In this model, we consider only the heterodimer Dpp/Scw and do not explicitly consider the homodimer counterparts Dpp/Dpp and Scw/Scw. However the results pertaining to extracellular patterning and positive feedback herein are easily extended to the homodimer counterparts, but the robustness will be significantly less for either Dpp or Scw homodimers [1]. The main result from (1-3) in [ref. 1] is that the system exhibits insensitivity at the level of Dpp/Scw for 2 fold changes in the level of Scw. Defining the dimensionless variables $u = \sqrt{K_2/\phi_W}X$, $v = \sqrt{K_3/\phi_W}Y$, $\Omega \equiv K_1/2\sqrt{K_2 K_3}$, $\beta \equiv \phi_D/\phi_W$ and choose $\Omega = 1/2$ gives:

$$\gamma_1[DW_{in}] = \phi_W^{wt} 2\Omega uv = \frac{\phi_D \phi_W}{\phi_D + \phi_W}$$

The input BMP to the PV space is then: $\frac{V_{in}}{V_{PV}} \frac{\phi_D \phi_W}{\phi_D + \phi_W}$. Here $V_{in}/V_{pv} = 1*10^{-3}$, $\phi_D = 1\mu M*min^{-1}$, and $\phi_W = 10\mu M*min^{-1}$. The output from this module provides the input to the second module, and there is no feedback to this module from later steps.

3 Module II: Extracellular pattern formation

Following secretion into the PV space, BMPs interact with extracellular BMP binding proteins Sog and Tsg (see main text: (Introduction) for a brief description). The evolution of the extracellular processes is given by five partial differential equations given at (4-8). The extracellular patterning model used herein is based upon our current understanding of interactions between regulators in the PV space. The extracellular component of this model is similar to those used previously to describe gradient formation during DV patterning [2, 3].

$$\frac{\partial[B]}{\partial t} = D_B \frac{\partial^2[B]}{\partial x^2} + \gamma_1 \frac{V_{in}}{V_{PV}}[DW_{in}] - k_3[I][B] + k_{-3}[IB] + \lambda[Tol][IB] - \delta_B[B]$$
$$+ R([B],[R],[C],...) \tag{4}$$

$$\frac{\partial[S]}{\partial t} = D_S \frac{\partial^2[S]}{\partial x^2} + \phi_S - k_2[S][T] + k_{-2}[I] - \delta_S[S] \tag{5}$$

$$\frac{\partial[T]}{\partial t} = D_T \frac{\partial^2[T]}{\partial x^2} + \phi_T - k_2[S][T] + k_{-2}[I] + \lambda[Tol][IB] - \delta_T[T] \tag{6}$$

$$\frac{\partial[I]}{\partial t} = D_I \frac{\partial^2[I]}{\partial x^2} + k_2[S][T] - k_{-2}[I] - k_3[I][B] + k_{-3}[IB] \tag{7}$$

$$\frac{\partial[IB]}{\partial t} = D_{IB} \frac{\partial^2[IB]}{\partial x^2} + k_3[I][B] - k_{-3}[IB] - \lambda[Tol][IB] \tag{8}$$

Here, extracellular BMP (Dpp/Scw) is denoted (B), Sog (S), Tsg (T), Sog/Tsg (I), and Sog/Tsg/Dpp/Scw (IB). ϕ_T, ϕ_S, and $\frac{V_{in}}{V_{PV}}DW_{in}$ are the secretion rates of Tsg, Sog, and BMP into the PV space respectively. Sog and Tsg bind reversibly to form I with constants k_2, and k_{-2} for the forward and reverse rates. BMP and I reversibly bind with forward and reverse constants k_3, and k_{-3}. R(B,R,C,...) denotes receptor/surface interactions and different cases for R will be analyzed in more detail later. The complex IB is degraded by Tolloid with rate λTol. Degradation cleaves Sog and releases Tsg and B. The extracellular components in this model undergo non-specific first order degradation/removal.

4 Module III: Receptor interactions and positive feedback

4.1 Receptor role in the formation and interpretation of the extracellular gradient

Formation of the extracellular BMP distribution involves a complex interplay between diffusion and a number of kinetic processes, and the balance between these processes changes along the DV axis. An important factor in localizing Dpp/Scw at the DM is the ability of Sog/Tsg to shuttle Dpp/Scw up the gradient of Dpp/Scw, which has its high point at the DM. Localization of Dpp/Scw at the DM would be enhanced by reducing its diffusion coefficient, and this strategy is used in Model I [2], where the diffusion constant of Dpp/Scw is set to zero. However, some controversy exists surrounding the zero diffusion assumption [3-5]. An alternative strategy is to enhance the degradation of Dpp/Scw, for this reduces the amount available for signaling, and since Dpp/Scw is highest at the DM, the signal is highest there. Of course this strategy has the energetic cost of turnover of the signal. A related strategy is used in Model II, in which extracellular BMP is not degraded directly, but rather, degradation is mediated by receptor binding [3]. To better understand these different strategies and how they depend on BMP degradation and receptors, it is helpful to first consider a simple representation of the processes involved, namely, diffusion, signal-independent production and first-order degradation, as given by the equation

$$\frac{\partial [B]}{\partial t} = D_B \frac{\partial^2 [B]}{\partial x^2} + r\left([B], [I], x, ...\right) - \delta B \tag{9}$$

Where (...) includes other model specific components. Scaling time by δ, x by the system length L and assuming B is order one leads to:

$$\frac{\partial [B]}{\partial \tau} = \theta \frac{\partial^2 [B]}{\partial \bar{x}^2} + \frac{r\left([B], [I], x, ...\right)}{\delta} - [B] \tag{10}$$

7

The dimensionless diffusion coefficient $\theta \equiv \frac{D_B/\delta}{L^2}$ is the square of the ratio of two characteristic lengths. The first, $\sqrt{D_B/\delta}$, is a characteristic diffusion length and measures the distance a molecule is spread by diffusion in unit time (measured here in units of the inverse decay rate of BMP), and the second is a characteristic length of the system. If $\sqrt{D_B/\delta}$ is small compared to L, the spread of free BMP is restricted to a small fraction of the domain since it degrades rapidly relative to the rate at which it spreads by diffusion, but if $\sqrt{D_B/\delta}$ is large relative to L, diffusion dominates and the signal spreads rapidly. Thus localization of the signal can be achieved either by having a small diffusion coefficient or a large degradation rate. In our model with linear degradation (no positive feedback) the diffusion length is approximately 65μ, and since the circumference is 550μ, this suggests that Dpp is moderately localized, which contributes to the sharp spatial gradient.

Next we examine the effect that receptors have on localization of BMPs and the receptor interpretation of BMP signal. In Case 1 we consider simple receptor binding dynamics, while in Case 2 we look at receptor-mediated degradation. These cases have no feedback. In Case 3, we study how positive feedback of a membrane-bound binding protein affects the interpretation of the BMP gradient with extracellular degradation of BMP. And lastly, in Case 4 we look at the model of the main text with positive feedback and endocytosis-mediated degradation of the BMP (Figure 7).

4.2   Receptor binding (Case 1)

The simplest interaction arises when BMP binds to the receptor at a rate k_{on} and is released at the rate k_{off}, and this leads to the following equations, wherein BR is the concentration of BMP-occupied receptor and B is the concentration of extracellular BMP.

$$\frac{\partial[B]}{\partial t} = D_B \frac{\partial^2[B]}{\partial x^2} - k_{on}[B]\left(R_{tot} - [BR]\right) + k_{off}[BR] + r\left([B], [I], x, ...\right) - \delta[B] \qquad (11)$$

$$\frac{\partial[BR]}{\partial t} = k_{on}[B]\left(R_{tot} - [BR]\right) - k_{off}[BR] \qquad (12)$$
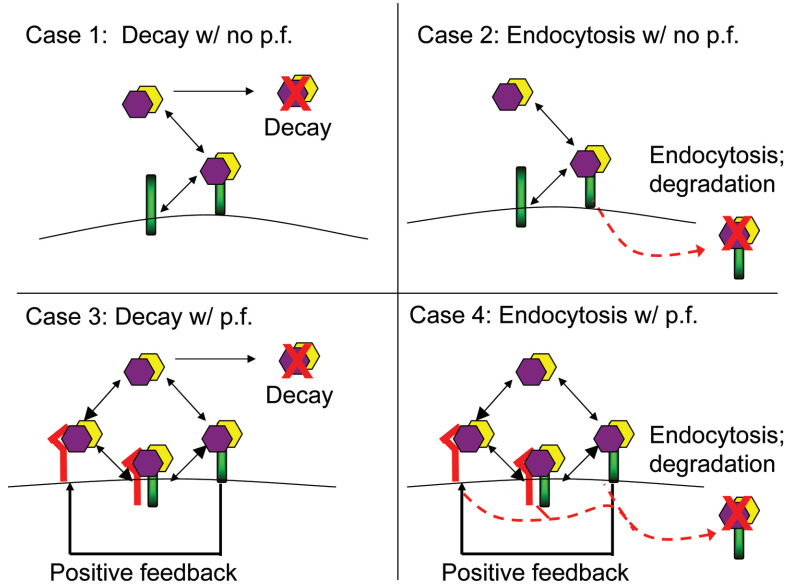
Figure 7: Different receptor models. Symbols are as in Figure 6.

Since receptor binding and release are fast relative to diffusion and other extracellular processes, we can assume a quasi-steady state for the BR binding steps, which yields $[BR] = [B] \bullet [R_{tot}]/([B] + k_{off}/k_{on})$. Thus the level of BR is proportional to the level of extracellular BMP for $[B] << k_{off}/k_{on}$, and saturates as B increases. When the extracellular concentration varies in time the receptors act as a capacitance to slow changes. However, at equilibrium the contribution is zero and therefore does not affect the steady-state distribution in space. This simple readout of the extracellular morphogen gradient can produce BR profiles that correspond generally well with pMad staining in the *Drosophila* embryo 8. Because the level of BR directly reflects the extracellular concentration of BMP, robustness present in the mechanism for establishment of the spatial profile feeds directly into BR.

4.3   Receptor-mediated degradation (Case 2)

Recently, a model that incorporated receptor-mediated degradation of BMP was developed (Model II)[3]. The governing equations are:
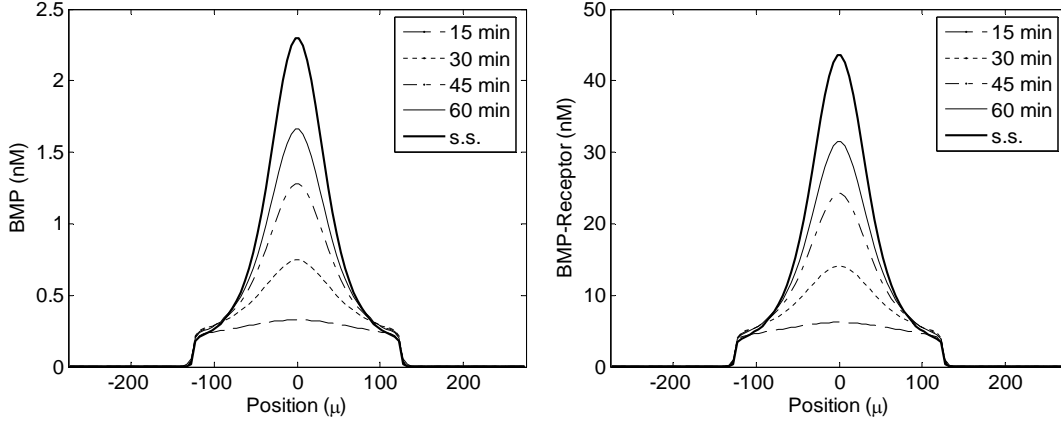
Figure 8: Transient evolution of BMP and BMP-Receptor for Case 1. The position 0 corresponds to the dorsal midline.

$$\frac{\partial [B]}{\partial t} = D_B \frac{\partial^2 [B]}{\partial x^2} - k_{on}[B]\left(R_{tot} - [BR]\right) + k_{off}[BR] + r\left([B],[I],x,...\right) \qquad (13)$$

$$\frac{\partial [BR]}{\partial t} = k_{on}[B]\left(R_{tot} - [BR]\right) - \left(k_{off} + k_{deg}\right)[BR] \qquad (14)$$

Here, R_{tot} is the total amount of surface-localized receptors and k_{deg} is the internalization rate of the BR complex. This equation is based on two features: very rapid intracellular processes, and as shown next, free and bound receptors internalize/degrade at the same rate.

If we denote the above species as R_s, R_i, R_sL, R_iL where R is receptor, s is cell surface, i is internal and L denotes ligand, the following set of ordinary differential equations can be derived.

$$\frac{d[R_S]}{dt} = -k_{on}[L][R_S] + k_{off}[LR_S] - k_{i1}[R_S] + \gamma[R_i] \tag{15}$$

$$\frac{d[LR_S]}{dt} = k_{on}[L][R_S] - k_{off}[LR_S] - k_{i2}[LR_S] \tag{16}$$

$$\frac{d[LR_i]}{dt} = k_{i2}[LR_S] - \lambda_L[LR_i] \tag{17}$$

$$\frac{d[R_i]}{dt} = \lambda_L[LR_i] + \phi_R - \gamma[R_i] + k_{i1}[R_S] - \lambda_R[R_i] \tag{18}$$

Also, ϕ_R is the production of receptor, k_{i1} and k_{i2} are the internalization rate for free and
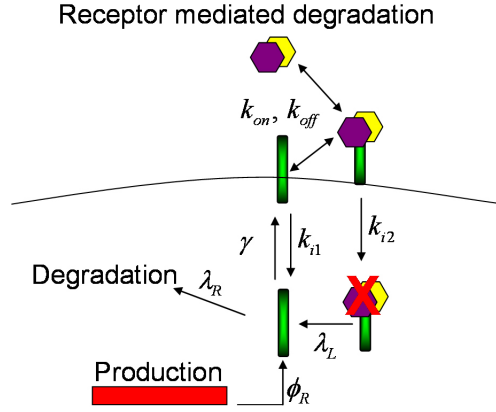
Figure 9: Receptor-mediated endocytosis.

bound receptors, and λ_L and λ_R are the ligand and receptor degradation rates respectively. If a quasi-steady-state for the internal processes is assumed, and if we impose a conservation condition on the level of receptors on the surface, then (15),(16)=0$\Rightarrow [LR_i] = \frac{k_{i2}}{\lambda_L}[LR_S]$ (17)+(18)$\Rightarrow \frac{d[R_S]}{dt} + \frac{d[LR_S]}{dt} = \frac{d[R_0]}{dt} = 0 = -k_{i1}[R_S] - k_{i2}[LR_S] + \gamma[R_i]$. Now sub (17) into (18) and arrive at $-k_{i2}[LR_S] - k_{i1}[R_S] + \gamma[R_i] = \phi_R - \lambda_R[R_i]$ and $[R_i] = \frac{\phi_R}{\lambda_R}$. This gives $k_{i1}[R_S] + k_{i2}[LR_S] = \frac{\gamma\phi_R}{\lambda_R}$. Now $0 = -k_{i1}([R_0] - [LR_S]) - k_{i2}[LR_S] + \gamma\frac{\phi_R}{\lambda_R}$ $k_{i1}\frac{d[R_0]}{dt} = 0 \Rightarrow 0 = (k_{i1} - k_{i2})\frac{d[LR_S]}{dt}$ and $k_{i1} = k_{i2}$.

Thus, receptor-mediated degradation of the form used in Model II implies that free and bound receptors internalize at the same rate. This has been shown in some contexts experimentally [6] and this result will be used later for derivation of the positive feedback

mechanism.

In this scheme BMP is removed from the extracellular space only when bound to receptor, and some simple assumptions make the role of receptor-mediated degradation more transparent. To identify an appropriate kinetic scale, note that there are two dominant kinetic processes that contribute to the localization of BMP: inhibitor binding/cleavage and receptor binding and degradation. Since the maximum signal range depends on the slowest kinetic process, we focus on the slower receptor internalization and degradation rather than the fast extracellular inhibitor binding. Furthermore, the BR off-rate used was $4 \cdot 10^{-6} \text{sec}^{-1}$ in [3] which is very small relative to many of the other kinetic rates (e.g. 100 fold smaller than the degradation rate) and can be assumed to be zero. Thus, the effective receptor-mediated removal rate of BMP from the PV space depends on the balance of receptors and the equation becomes:

$$\frac{\partial [B]}{\partial t} = \underbrace{D \frac{\partial^2 [B]}{\partial x^2}}_{Diffusion} - \underbrace{f\left([BR]\right)[B]}_{Rec.Rem.} + \underbrace{k_{off}[BR]}_{\sim \vartheta(0)} + \underbrace{r([B],[I],x,...)}_{Binding,...} \tag{19}$$

The characteristic degradation parameter $\delta = f(BR)$ depends upon the level of BMP bound to receptor. Due to the fast binding steps coupled with the slower release and degradation of BMP, the quasi steady-state analysis cannot be invoked *a priori* so we first analyze the transients for the level of BR. Suppose B varies slowly on the binding time scale variable so that receptors perceive it as constant, then:

$$[BR](t) \approx \frac{\alpha}{\beta} \left(1 - \exp\left[-\beta t\right]\right), \quad \alpha = k_{on}[R_0][B], \quad \beta = k_{on}[B] + k_{off} + k_{deg}$$

The approximate time for BR to reach 80% of its equilibrium value for BMP near the midline is $\ln(0.2)/-\beta \approx 1.5\,\text{min}$ or 2.3 min to reach 90% of it's equilibrium value. For lower levels of BMP, the time to equilibrate is slower, taking on the order of 5 minutes. Since the level of BMP is increasing in the PV space during patterning in this model [3], the level of BR lies somewhere between zero and the steady-state level. For early transient patterning, before receptors equilibrate, the 1st order removal of BMP from the extracellular space (δ)

is $\delta \sim k_{on}[R_0] = 1.2\text{sec}^{-1}$. At steady-state the removal rate of BMP from the PV space is $\delta \sim (k_{deg}k_{on}[R_0])/(k_{on}[B] + k_{off} + k_{deg}) = 0.04\text{sec}^{-1}$. These values for the effective 1st order removal rates give diffusion lengths $\sqrt{D_L/k}$ between 8μ and 45μ. Since the circumference of the embryo is $\sim 550\mu$, this means that the BMP localized by other mechanisms will travel only a very short distance before being bound by receptor and degraded, thus localizing it in the presence of diffusion. The analysis of robustness for this receptor interaction is analyzed in detail in Mizutani et al. [3] and in section 7 herein.
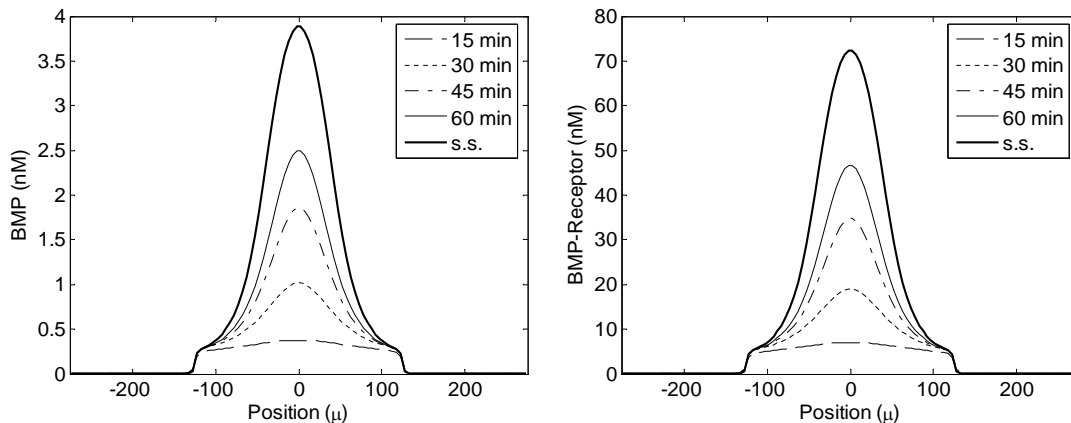
Figure 10: Transient evolution of model with receptor mediated endocytosis of BMP.

4.4 Derivation of local dynamics for positive feedback of SBP

In this section we provide further details on two cases that may lead to the positive feedback identified by Wang and Ferguson [5]. A candidate molecule of BMP receptor activation is a membrane bound BMP binding protein. Figure 11 shows the full proposed mechanism for receptor activation and signaling.

In Case 3, the SBP is degraded in all forms at a rate δ_D, but receptor is not ($\delta_E = 0$). BMP-bound SBPs release BMP upon degradation and as a result, positive feedback does not influence the extracellular BMP distribution at steady-state. This mechanism biologically resembles secretion of a molecule that binds extracellular components that restrict its

movement (perhaps by binding to heparin-sulfate proteoglycans) but is not specifically endo-cytosed. Case 4 involves endocytosis of BMP when bound to SBPs (or receptors) associated with the membrane which internalize at the rate δ_E before undergoing intracellular degra-dation and/or recycling. For simplicity we assume that BMP decays only in the unbound state, thus the total rate of removal of BMP is the sum of the extracellular decay and the surface-associated endocytosis. The difference between these cases stems principally from the fact that in Case 3 BMP is not lost as a result of binding, while Case 4 leads to a loss of BMP via endocytosis. The latter couples the steady-state distribution of SBP and BMP in the PV space.

The simplified mechanism presented in the main text can easily be derived by making a few assumptions. First, the level of receptor complex composed of type I and type II receptors forms by binding of BMP to one type of receptor, which facilitates the recruitment of the other receptor to form an active signaling complex. Once the complex is formed, it starts phosphorylating Mad. If Mad is not limiting, the production of pMad is proportional to the number of bound receptors. Once phosphorylated, pMad binds to the co-Smad Medea before translocating to the nucleus to control target genes. Since the binding of pMad to Medea is an example of a dimerization step of the type analyzed in detail previously [1], two cases are possible. In one case, the level of Medea exceeds the level of pMad and the level of pMad bound to Medea is directly proportional to the level of pMad in the system. In the case with limiting Medea, the formation of the complex saturates as the level of pMad increases and the difference between bound states of receptors would be dampened out. For the analysis here, we only look at the case in which Medea is in excess and the level of the pMad/Medea complex is directly proportional to the level of ligand bound receptors (i.e. pMad/Medea$\sim \alpha$*ActiveReceptor). Gene expression is modeled using a second order Hill function similarly used in other systems with positive feedback. If a constant level of surface receptors for the case with the positive feedback of the BMP binding protein, we obtain a similar expression and requirement for the internalization rate of the various components as

Figure 11: Schematic representation of SBP action.

derived earlier for Case 2. Here the condition that must be satisfied is:

$$0 = (k_{i1} - k_{i2})\frac{d[BR_S]}{dt} + (k_{i1} - k_{i3})\frac{d[CBR_S]}{dt}$$

where C denotes the SBP, R_S is the surface localized receptors, and B is the BMP. This condition is easily satisfied by setting all the internalization rates equal. For simplicity, we set the internalization rate for the free and BMP-bound surface binding proteins equal to the receptor internalization rate for the computations.

The active signaling complex for BMPs is composed of both type I and type II BMP receptors. The equations for the full patterning model are:

$$\frac{d[C]}{dt} = \frac{\Lambda \cdot [BRP]^\nu}{K_{h1}^\nu + [BRP]^\nu} - k_4[B][C] + k_{-4}[BC] - k_7[BR][C] + k_{-7}[BCR]$$
$$- (\delta_D + \delta_E)[C] \tag{20}$$

$$\frac{d[BC]}{dt} = k_4[B][C] - k_{-4}[BC] - k_6[BC][R] + k_{-6}[BCR] - (\delta_D + \delta_E)[BC] \tag{21}$$

$$\frac{d[BCR]}{dt} = k_6[BC][R] + k_7[BR][C] - k_{-6}[BCR] - k_{-7}[BCR] - (\delta_D + \delta_E)[BCR] \tag{22}$$

$$\frac{d[BR]}{dt} = k_5[B][R] - k_{-5}[BR] + (k_{-7} + \delta_D)[BCR]$$
$$- k_7[BR][C] - k_8[BR][P] + k_{-8}[BRP] - \delta_E[BR] \tag{23}$$

$$\frac{d[BRP]}{dt} = k_8[P][BR] - (k_{-8} + \delta_E)[BRP] \tag{24}$$

$$[R_{tot}] = [R] + [BR] + [BCR] + [BRP], \quad [P_{tot}] = [P] + [BRP] \tag{25}$$

where, B denotes BMP, R denotes the type I receptor and P denotes the type II receptor. At steady-state, the level of BRP is

$$[BRP] = \frac{[P_{tot}][BR]}{[BR] + (k_{-8} + \delta_E) / k_8} \tag{26}$$

which for BR ($[BR] << (k_{-8} + \delta_E)/k_8$),

$$BRP \approx (k_8/(k_{-8} + \delta_E))P_{tot}BR = K_{eq} \cdot BR \tag{27}$$

In the positive feedback model this primarily affects the level of free receptor that can participate in binding reactions with other components. For simplicity, assuming the level of BRP is small relative to R, BR, and BCR, the following equations were used:

16

$$\frac{d[C]}{dt} = \frac{\Lambda[BR]^\nu}{K_h^\nu + [BR]^\nu} - k_4[B][C] + k_{-4}[BC] - k_7[BR][C] + k_{-7}[BCR]$$
$$- (\delta_D + \delta_E)[C] \tag{28}$$

$$\frac{d[BC]}{dt} = k_4[B][C] - k_{-4}[BC] - k_6[BC][R] + k_{-6}[BCR] - (\delta_D + \delta_E)[BC] \tag{29}$$

$$\frac{d[BCR]}{dt} = k_6[BC][R] + k_7[BR][C] - k_{-6}[BCR] - k_{-7}[BCR] - (\delta_D + \delta_E)[BCR] \tag{30}$$

$$\frac{d[BR]}{dt} = k_5[B][R] - k_{-5}[BR] + (k_{-7} + \delta_D)[BCR] - k_7[BR][C] - \delta_E[BR] \tag{31}$$

$$[R_{tot}] = [R] + [BR] + [BCR] \tag{32}$$

and in terms of K_{eq}, $K_h^\nu = K_{h1}^\nu/(K_{eq})^\nu$.

4.5   Positive feedback with extracellular decay (Case 3)

In this case, unbound extracellular BMP undergoes first-order degradation at a rate $\delta_B = 1$ min^{-1}, and the SBPs decay at a rate $\delta_D = 0.03$ min^{-1} and $\delta_E = 0$. At steady-state the positive feedback and receptor interactions sum to zero and therefore do not affect the shape of the extracellular morphogen gradient. Plotting the point wise data for extracellular BMP vs. the level of BR on the equilibrium diagram for the local dynamics shows that this mechanism leads to a threshold response to a time-independent distribution of BMP; some cells lie near the lower branch while others lie near the upper branch, and the transition occurs between two adjacent cells (Figure12 a). The threshold level of BMP corresponds to the limit point of the equilibrium curve: cells that detect BMP above that level eventually adopt a high signaling cell fate, while cells below that point adopt a low signaling fate. With this mechanism, two very different extracellular BMP profiles can lead to approximately the same profile of BRs. To demonstrate this, we reduced the binding affinity of Dpp/Scw to Sog/Tsg and lowered the decay rate so the extracellular gradient is broad (dashed line, Figure 12 c). In Figures 12 b and 12 c, the extracellular gradients have a very different

shape, but the level of BRs is very similar, differing primarily in amplitude near the midline. Since the extracellular ligand distribution is determined independently of positive feedback interactions, the robustness results from earlier models translate directly into the level of BR and thus to signaling at steady-state.
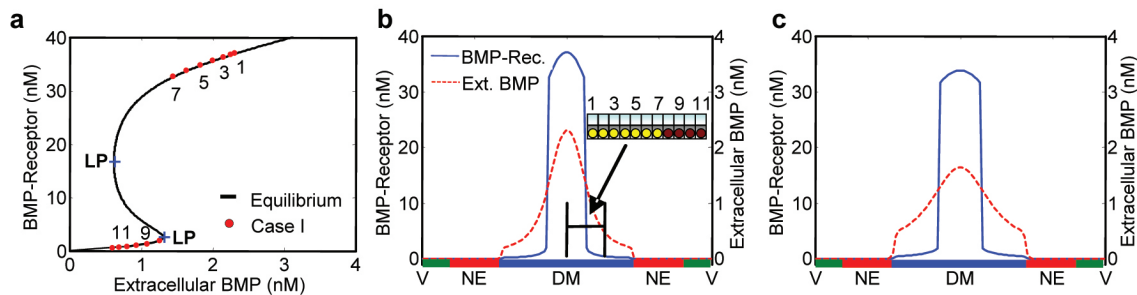
Figure 12: Case 3, no endocytic degradation. (a-c) Positive feedback leads to spatial bistability. (a) The steady-state response, as measured by the level of BR as a function of extracellular BMP, treated as a parameter. For low BMP, BR interactions closely follow the binding curve. When the level of extracellular BMP exceeds the lower limit point (purple star), the lower branch disappears and the level of BR approaches the upper branch. Red dots are the level of BMP and BR corresponding to "cell positions" in the PV space (b). (b-c) Decay mediated removal of BMP and binding protein leads to a threshold response at steady-state. (b) BMP (dashed line; right axis) and the level of BR (solid line; left axis) vs. position at steady-state. (c) Same as in (b) except that the extracellular BMP is less tightly localized and higher throughout by setting $\delta_B = 9.2 \cdot 10^{-1} \text{min}^{-1}$ and $k_3 = 1.71$ nM^{-1}min^{-1}. The level of BR output in (b-c) is very similar in width and varies slightly in amplitude.

4.6   Positive feedback with endocytosis (Case 4)

Positive feedback acts at two levels to control the transient evolution of patterning. First, it enhances the binding of BMP to the receptor by increasing the local concentration of BMP that has access to receptors. Second, since we hypothesize that SBP/BMP complexes internalize, this creates a transient sink for BMP binding. Effectively, this gives a diffusion length for the system that changes in time. Initially, receptor mediated endocytosis (as in Case 2 above) limits the spread of free BMP. Once SBP is secreted, additional BMP binds to the SBP in addition to the receptors and removed from the PV space. This produces a transiently decreasing diffusion length, which leads to a gradient contraction. Other mech-

anisms that also lead to a contracting gradient are time-dependent BMP production [2], time-dependent Sog production or a transient inhibition of the Tld protease (unpublished data).
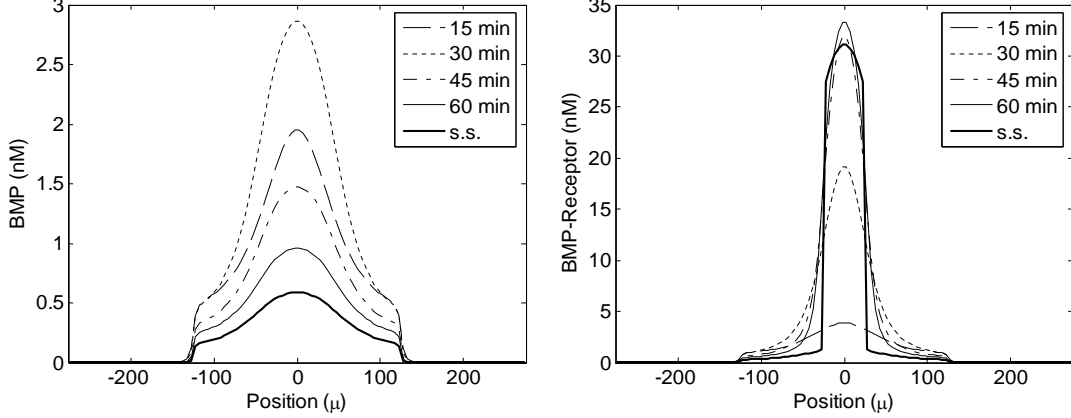
Figure 13: Transient evolution of model with positive feedback coupled with endocytosis of receptors and SBP (Case 4). Here, R_{tot}=320nM (see section 7 for explanation).

4.7   Decay and endocytosis (Composite of Case 3 & 4).

Here we expand the discussion of Cases 3 & 4 from the main text and analyze the transient evolution of the level of BR for intermediate systems in which both processes contribute (with varying degree) to the full patterning process. To do this, we have to balance the total degradation so that the number of cells that reach the upper branch (5-7) corresponds to the half-width of high intensity pMad signaling. First, we require that the sum of the degradation rates for decay and endocytosis of the binding protein remain constant (i.e. $\delta_D + \delta_E = \delta_{tot}$ = 0.03 min^{-1}) so that the level of SBP is consistent. Furthermore, since the protein decay process releases BMP while the endocytosis process removes BMP from the system, we scale the first order decay rate of extracellular BMP by the total (i.e. $\delta_{Beffective}$= (δ_D/δ_{tot})*δ_B) and then the level of extracellular BMP degradation interpolates between the maximum δ_B in the decay only case and zero in the endocytosis only case. To understand how the system responds to the intermediate ratios of the different removal processes, we plotted the transient

evolution of the level of BMP and BR above each cell as described in the main text for Figure 3 c. Figure 14 shows the results for four different ratios of the decay processes. Figure 14 a shows the case with only extracellular decay processes and the transient approach to the upper stable branch for the threshold mechanism (Case 3). The process is very slow because extracellular BMP levels are relatively low even though they exceed the limit point. Since the levels are low, the production of the binding protein in the positive feedback is slow and the evolution of BR to the upper stable branch is slow (much slower than embryonic patterning observed *in vivo*). Increasing the relative ratio of endocytosis to decay increases the rate at which cells approach the upper branch. Furthermore, this process feeds back into the extracellular patterning system, causing some cells that initially exceed the lower limit point to transiently return to the lower stable solution branch, since other competing cells begin removing the BMP from the extracellular space at a rapid rate. This leads to an initial broad distribution followed by a contraction. While the patterning time is slightly faster here, the positive feedback is still too slow to affect the pMad distribution and embryonic patterning. By further reducing the proportion of BMP removed by extracellular decay, the features previously noted become more pronounced. The fastest transient evolution with positive feedback occurs for Case 4 in which BMP is only removed by endocytosis when bound to either receptors or the SBP.

Also, Case 3 does not lead to a contraction at steady-state since all cells that sense an extracellular level of BMP that is greater than the lower limit point eventually reach the upper stable branch (Figure 14 a). As BMP is removed via endocytosis as in Case 4, some cells return to the lower equilibrium branch due to the rapid uptake of extracellular BMP by competing cells (Figure 14 b-d).
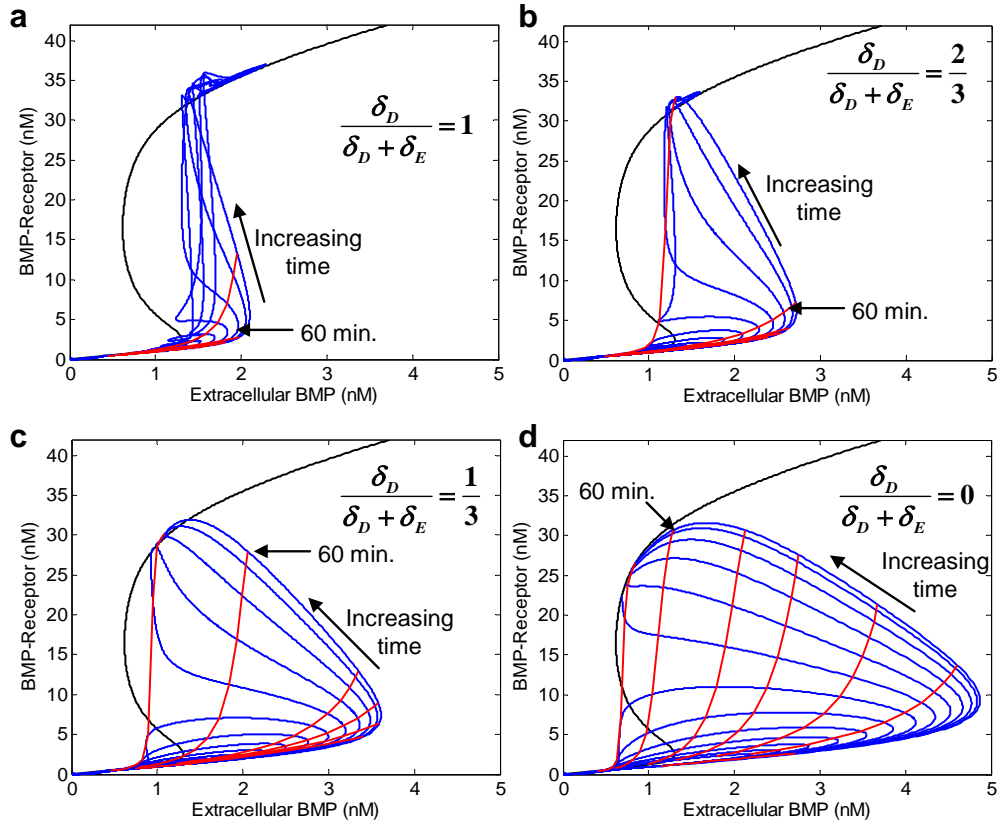
Figure 14: Homotop between Case 3 and Case 4.

4.8 Positive feedback time lag

Up to this point it was assumed that the transcriptional lag time for positive feedback is zero. However, it may be the case that signaling, gene control, and production of the SBP may have a lag time that may change both the transient evolution and steady-state distributions of patterning. To account for the positive feedback lag, changes were made in the equation

for SBP by introducing the term $(t - \tau)$.

$$\frac{d[C]}{dt} = \frac{\Lambda[BR]^\nu}{K_{h1} + [BR]^\nu}(t - \tau) - k_4[B][C] + k_{-4}[BC] - k_7[BR][C] + k_{-7}[BCR]$$
$$- (\delta_D + \delta_E)[C] \tag{33}$$

Here τ is a generic lag time that is specified as a parameter and this is commonly used in transient models with positive feedback. To compute transient patterns with the time lag, we programmed a delay differential equation (DDE) solver in Matlab and computed evolutions for long times. Figure 15 shows the transient trajectories of dorsal cells for $\tau = 0, 5$ and 10 min.

As the time lag associated with positive feedback is increased, there is significantly higher extracellular BMP during the transient evolution (compare Figure 15 a with b and c) along with a delay in the transient contraction. As patterning commences, the contraction is more pronounced for greater time-lags, however the time-scale for patterning becomes too long to be biologically meaningful. This suggests that either the positive feedback lag during patterning is small, or that the time-scale for the modeled system is incorrect for the specified set of parameters. The time-scale limiting parameter for the current model is the endocytosis rate δ_E which is based on earlier studies [3]. Our analysis suggests that when this constraint is relaxed, and faster endocytosis rates are used, the transient evolution can occur in the required time-scale even with a transcription time-lag (unpublished data).

5   Parameter values

The concentrations of the BMPs, inhibitors, and proteases are not precisely known. Parameter values were estimated based on in vitro experimental data, biacore binding data, and other sources.

Inhibitor binding parameters(k_2, k_{-2}, k_3, k_{-3}).   The binding parameters used are in the biologically reasonable range and based on previous studies where available. Furthermore, as
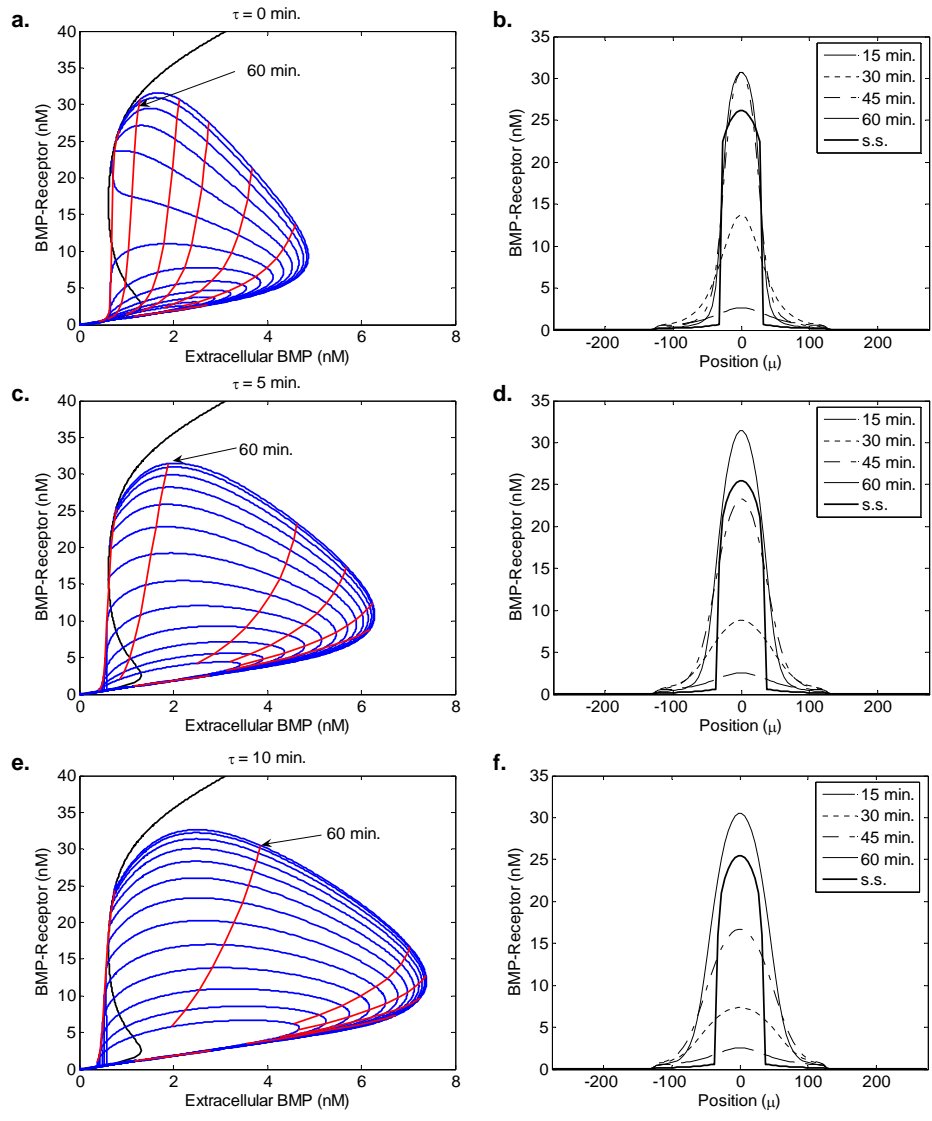
Figure 15: Effect of a transcription/production lag on patterning. Results are shown at for 0 min. (a,b), 5 min. (c,d) and 10 min. lag times (e,f).

shown later, the dynamics of the model do not depend on the specific choices of parameters and the model is insensitive to a large number of parameters when varied independently over 3 orders of magnitude (see section 7.2). The Sog and Tsg forward binding rate and the maximum value for B and I forward binding were approximated from previous work on extracellular BMP patterning and are given in Table 1 [3].

Receptor levels and SBP Production. The concentration of receptors that participate in transmitting the BMP signal from the PV space to the nuclei is unknown. The average number of receptors in 12 different cell types is approximately $1.2 \cdot 10^5$ receptors with a range of $9 \cdot 10^2$ to $7.1 \cdot 10^5$[7]. For example, there are $\sim 5 \cdot 10^3$ activin receptors per cell in the *Xenopus* blastula [8]. The area that each responding nucleus in the syncytium has exposed to the PV space is approximately a 5μ X 5μ patch of the PV membrane or approximately $1/6^{th}$ its total surface area. This gives a range of receptor numbers in the PV space of 150 to $1.2 \cdot 10^5$ receptors per nucleus. The volume of the PV space per nucleus is $\approx 12.5\mu^3$ and the receptor concentration can be computed by $R_{tot} = \rho/(V N_A)$ where ρ is the number of receptors, V is the volume, and N_A is Avogadro's number ($6.02 \cdot 10^{23}$). This gives a range of receptor concentration between 39 and $1.6 \cdot 10^4$ nM.

The maximal production rate of the SBP (Λ) was set at 180 molecules/cell/minute which corresponds to 24nM*min^{-1} which is in the same order of magnitude for receptor production rates used in similar studies [7, 9].

BMP and inhibitor levels. Using cell-based signaling assays, Shimmi and O'Connor demonstrated that *Drosophila* line S2 cells respond to Dpp concentrations <1nM [10]. In fact, pMad signaling observed in S2 cells changes from basal levels when Dpp concentration is 10^{-11} M to maximal expression when Dpp concentration is 10^{-9} M. While this information suggests signaling can occur at very low concentrations of Dpp, this does not guarantee concentrations *in vivo* are in the nM range. Nevertheless, the cell-based signaling assay provides an estimate for the concentrations of BMP species.

Second, it was shown that *in vitro* cleavage reactions exhibit the same dose dependency

observed in the cell-based signaling assays. When Sog was incubated with Tld and Dpp, strong proteolytic processing occurs at Dpp concentrations of 1nM. Furthermore, the *in vitro* reaction cleaves fragments off Sog after 15 minutes when incubated with $3 \cdot 10^{-10}$M Tsg and Dpp. Patterning time for the amnioserosa takes about 30-45 min. *in vivo* which is comparable with the time cleavage takes *in vitro*. These experiments provide evidence that suggests concentrations for BMPs and Tsg *in vivo* may be in the 1-10 nM range.

Sog production (ϕ_S) was set to 400nM*min^{-1}, while Tsg production(ϕ_T) is set to 36nM*min^{-1}. ϕ_D and ϕ_W are given in section 2. The level of extracellular Tld is fixed at 6nM. From section 2, The input BMP to the PV space is: $\frac{V_{in}}{V_{PV}} \frac{\phi_D \phi_W}{\phi_D + \phi_W}$. Here $V_{in}/V_{pv} = 1*10^{-3}$, $\phi_D = 1\mu$M*min^{-1}, and $\phi_W = 10\mu$M*min^{-1}. On a concentration basis, this gives heterodimer BMP inputs into the PV space on the order of 1nM*min-1.

In Case 3, the 1st order degradation/internalization for the BMP (δ_B)is set at 1.0min^{-1}. This is fairly rapid and gives a diffusion length of 66nM.

Diffusion coefficients. The simplest correlation based on the molecular weight, temperature, and solution viscosity provides a starting point for estimation of the diffusion of the species within the PV space. The equation relating temperature (T), viscosity (cP) and molecular weight (g mol^{-1}) is shown below [11].

$$D = 8.34 \bullet 10^{-8} \left(\frac{T}{\eta M^{1/3}} \right) \qquad cm^2 \ sec^{-1} \tag{34}$$

Using this equation, the diffusion constants for the species involved were calculated assuming 1 cp for the viscosity of water and 298 ^{o}K for T. The MW and calculated diffusion rate for the green fluorescent protein (GFP) is also calculated using the same equation. GFP, a 238 amino acid, 27 kD protein has an experimentally-determined diffusion coefficient of 85 μ^2 sec^{-1} in water. Thus for GFP, the equation yields an error of approximately 3.5%.

Receptor binding parameters. With low levels of morphogen in the PV space, it would seem that the ligand binding rate to receptor would have to be very high to ensure occupancy sufficient to signal. However, previous analysis suggested that in order for a suitable

gradient to form by diffusion, the forward step in binding has to be relatively low to ensure patterning is not too steep and acts over a range to be biologically useful [12]. In Drosophila embryonic patterning, the morphogen gradient begins broad and low and refines to a narrow stripe near the dorsal midline, which is the opposite of what occurs in classical morphogen gradient models where the gradient originates at secreting cells and extends through the developmental field by diffusion or other processes. In this context a rapid forward rate would limit the spread of BMP, but this would also have the negative effect of binding BMP and degrading it before the extracellular transport machinery effectively translocated the BMP from its region of expression to the dorsal midline [3]. In fact, the binding on-rate of BMP2 (Dpp like) to BMP Type I Receptors (BRIA) (Tkv like) is relatively slow with a k_{on} between $1.8 \cdot 10^{-2}$ nM^{-1}min^{-1} and $3.0 \cdot 10^{-2}$ nM^{-1}min^{-1} and the value used herein for the forward rate binding of the heterodimer Dpp/Scw (k_5) was $2.4 \cdot 10^{-2}$nM^{-1}min^{-1} [13, 14]. Typical dissociation constants (K_d) for BMP-2 with receptors is relatively high: $K_d \approx 1\,nM$ (Biacore) for the immobilized BMPR-IA ectodomains or 50 nM for the immobilized BMP-2 [14]. Another study found that BMP-2 binding with Tkv receptor also has a higher affinity with immobilized receptor (3.6 nM) versus (200 nM) for immobilized BMP-2 [13]. This suggests that for BMP-2 homodimer binding, the expected off-rate (if an on-rate of $2.4 \cdot 10^{-2}$nM^{-1}min^{-1} is assumed) is between $2.4\cdot 10^{-2}$min^{-1} and 4.8min^{-1}. The discrepancy in K_d values for the two different immobilized factors may be caused by two immobilized receptors binding to a single ligand, which may be the more biologically relevant case. Since the ligand involved in *Drosophila* patterning is likely a heterodimer of Dpp/Scw [1], binding rates of the Scw like BMP-7 were estimated. Receptor binding of BMP-7 (Scw like) to type I BMP receptors is significantly lower with K_d values for immobilized receptor that are either medium $K_d = 2 - 10nM$ or low $K_d = 10 - 100nM$ [14]. However, at this time it is unclear if the low K_d values is caused by a slower on-rate or a faster off rate. In the modeling of receptor interactions, the details of oligomerization and heterodimer formation were not considered. For additional analysis of heterodimer formation see Shimmi et al. [1] or Vilar et al. [15]. A relatively fast off rate (k_{-5})of 4min^{-1} which gives a $K_d \approx 166$nM was used for the calculations in the main text. See section 7 on parameter sensitivity for additional

discussion.

Surface bound BMP binding protein (SBP) binding parameters. Without the identity of the molecule in the embryonic context that leads to accumulation of BMP at the dorsal surface we can only speculate on appropriate parameter values or even a range of parameter values appropriate for modeling. In the analogous patterning stage during zebrafish gastrulation [16] and during BMP patterning of the pupal wing (our unpublished data) Crossveinless-2 (Cv-2) is the positively regulated component required to potentiate BMP signaling. The binding affinity of BMP-2 for WT Cv-2 is $K_d \approx 1.4$nM with an on-rate of $\approx 1.4 \cdot 10^{-1}$nM^{-1}min^{-1} and an off-rate of $\approx 1.9 \cdot 10^{-1}$min^{-1} [16]. For BMP-7 the $K_d \approx 3.5$nM with an on-rate of $\approx 1.4 \cdot 10^{-1}$nM^{-1}min^{-1} and an off-rate of $\approx 4.7 \cdot 10^{-1}$min^{-1}. The on-rate for both BMP-2 and BMP-7 is about 6-8 fold higher for Cv-2 than for receptor which would lead to accumulation of BMP in regions with high levels of Cv-2. An on-rate (k$_4$) of 1nM^{-1}min^{-1} and an off-rate (k$_{-4}$) of 2 min^{-1} with a $K_d = 2$nM were used in the absence of the aforementioned data regarding Cv-2, however if the above rates are used for Cv-2, there is little effect on the transient evolution or steady-state properties of the BMP-receptor distribution (our unpublished data).

The rates for the transfer of BMP between SBP and receptors on the surface are largely unknown at this time and rates were chosen in the biologically feasible range for k$_6$, k$_{-6}$, k$_7$, and k$_{-7}$. The model behavior is largely insensitive to these choices as shown in section 7.

5.1   Numerical methods

In view of assumption 3, the steady-state versions of equations 1-3 were solved using the results for general heterodimer formation [1]. Equations 4-8 were solved for various receptor models using the finite difference method on an axial cross-section halfway between the anterior and posterior poles. The equations were solved on half the circumference of the cross-section by imposing symmetry conditions at the dorsal and ventral midline. We used 55 node points in the half-width, which is approximately the number of prospective cells. In this way, we treat each node point as a cell lining the PV-space and are able to track the

Name	Description	Value	Units	Figure
Ω	Dimer formation	0.5	$Dimensionless$	
γ_1	Secretion Rate	arbitrary	sec^{-1}	
	Inhibitor Binding			
k_2	Binding Sog/Tsg	$3.0 * 10^{-1}$	$nM^{-1}min^{-1}$	25
k_{-2}	Reverse	$1.8 * 10^0$	min^{-1}	25
k_3	Binding I to B	$5.7 * 10^0$	$nM^{-1}min^{-1}$	26
k_{-3}	Reverse	$1.8 * 10^{-1}$	min^{-1}	26
	Receptor/SBP Binding			
k_4	Binding B to C	$1.0 * 10^0$	$nM^{-1}min^{-1}$	22,23
k_{-4}	Reverse	$2.0 * 10^0$	min^{-1}	22,23
k_5	Binding B to R	$2.4 * 10^{-2}$	$nM^{-1}min^{-1}$	21,23
k_{-5}	Reverse	$4.0 * 10^0$	min^{-1}	21,23
k_6	Binding BC to R	$5.0 * 10^{-1}$	$nM^{-1}min^{-1}$	22,23
k_{-6}	Reverse	$1.0 * 10^1$	min^{-1}	22,23
k_7	Binding BR to C	$1.3 * 10^{-1}$	$nM^{-1}min^{-1}$	22,24
k_{-7}	Reverse	$1.0 * 10^1$	min^{-1}	22,24
	Diffusion			
D_S	Diffusion, Sog	50	$\mu^2\ sec^{-1}$	27
D_T	Diffusion, Tsg	66	$\mu^2\ sec^{-1}$	27
D_B	Diffusion, BMP	73	$\mu^2\ sec^{-1}$	27
D_{IB}	Diffusion, I/BMP	42	$\mu^2\ sec^{-1}$	27
D_I	Diffusion I	45	$\mu^2\ sec^{-1}$	27
	Production, etc.			
ϕ_S	Sog secretion	400	$nM*min^{-1}$	
ϕ_T	Tsg secretion	36	$nM*min^{-1}$	
ϕ_D	Dpp production	1	$\mu M*min^{-1}$	
ϕ_W	Scw production	10	$\mu M*min^{-1}$	
V_{in}/V_{pv}	Volume ratio	$1.0 * 10^{-3}$	$Dimensionless$	
Tld	Tld levels	6	nM	
R_{tot}	Total Receptor Level	160, 320*	nM	
	Degradation			
λ	Tld process rate	$5 * 10^0$	$nM^{-1}min^{-1}$	
δ_{Sog}	Sog Degrade	$1.5 * 10^{-1}$	min^{-1}	
δ_{Tsg}	Tsg Degrade	$5.0 * 10^{-2}$	min^{-1}	
δ_B	B Degrade	$1.0 * 10^0$	min^{-1}	
$\delta_{tot}, (\delta_E)$	Membrane Prot. Degrade	$3.0 * 10^{-2}$	min^{-1}	
	SBP production			
Λ	Bind. Prot. Production	24	$nM*min^{-1}$	24
K_H	Hill parameter	31.63	nM	24
ν	Cooperativity/Gene Param.	2	$Dimensionless$	24

Table 1: Model parameters. The figure column lists the figure(s) where parameters underwent sensitivity analysis. * denotes R_{tot} used for Case 4 in section 7.2. and Figure 2 in main text

transient behavior of individual cells on standard bi-stability diagrams. Bifurcation diagrams corresponding to the local dynamics of the positive feedback loop were calculated using the software Matcont written for Matlab [17].

6 Transient evolution of patterning components

The primary focus of the analysis and article is on the distribution of BMP bound to receptor. However, BR depends upon the distribution of many other patterning components which are given in Figures 16 and 17.

7 Parameter sensitivity and robustness

7.1 Upstream mechanisms of robustness.

It is found experimentally that D/V patterning is surprisingly robust with respect to reductions in the levels of many of the components. For instance, the width of the pMad expression domain is insensitive to reductions in the level of extracellular components Tsg, Scw, and Tld [2] while it shows greater sensitivity to reductions in Sog [3]. Patterning is highly sensitive to changes in the level of Dpp. Earlier analysis of extracellular BMP patterning (Module II) demonstrated that for certain sets of parameters, the computational system exhibits "robustness" or insensitivity to 2-fold changes in the levels of Sog, Scw, and Tld at steady-state [2]. The conditions for steady-state robustness are (1) BMP dependent processing of Sog by Tld; (2) free BMP molecules do not diffuse independently; (3) BMPs bind irreversibly to receptors; (4) Sog can remove BMP from receptors, and (5) Dpp and Scw patterning is decoupled by the Sog/Tsg complex. While condition 5 is not met since patterning is likely mediated by a heterodimer Dpp/Scw [1] conditions (1-4) should be considered separately. The net effect of conditions (1-4) is to strongly localize BMP in the absence of Sog binding. That BMPs are localized in the absence of the inhibitor Sog has become controversial since new findings suggest that Dpp can act over 15-20 cell diameters and Scw can act over even
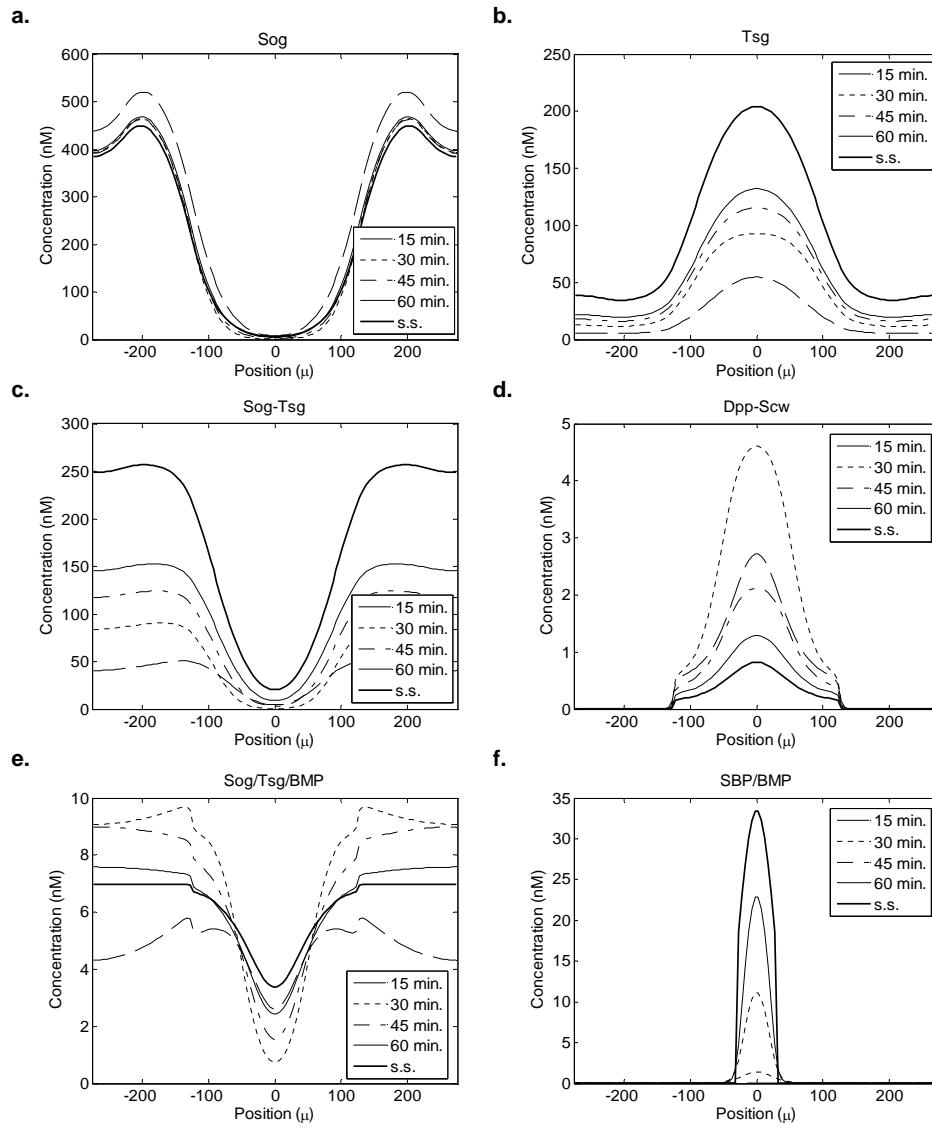
Figure 16: Transient evolution of Sog (a), Tsg (b), Sog/Tsg (c), Dpp/Scw (d), Sog/Tsg/Dpp/Scw (e), and SBP/BMP (f).
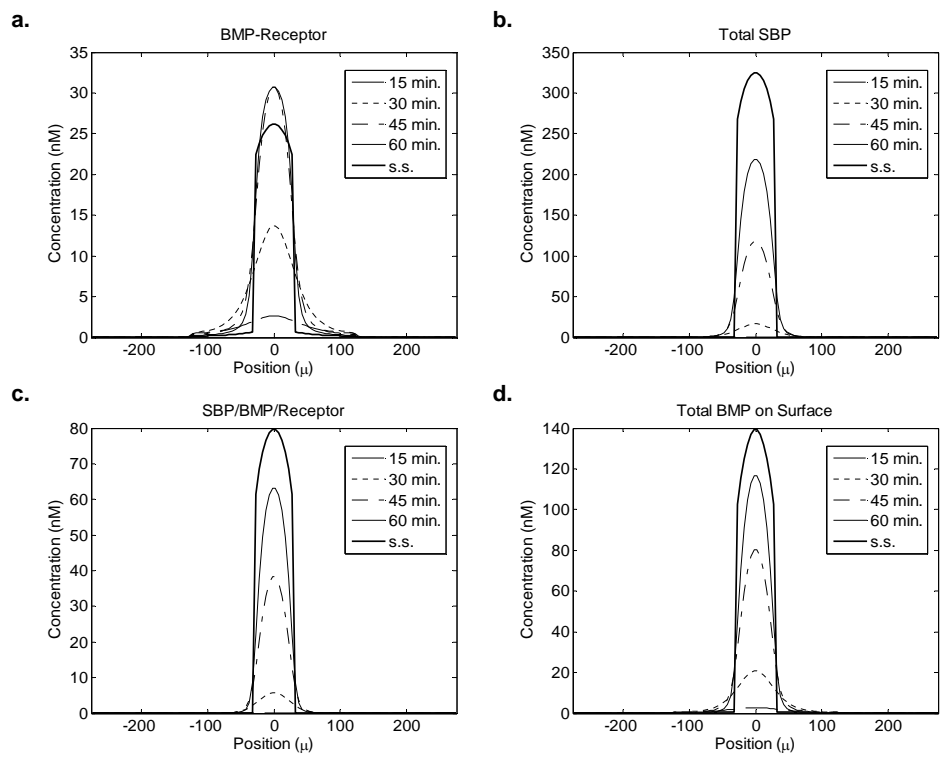
Figure 17: Transient evolution of BMP-Receptor (a), Total SBP (b), SBP/BMP/Receptor (c), and total BMP on surface (d).

greater distances [3, 5]. However, using PVI staining of Dpp-GFP, it was also shown that over time, BMP is immobilized on the surface and accumulates in a narrow region near the dorsal midline [5], presumably as the result of binding to either receptors or another factor such as an SBP. This suggests that the diffusibility of BMP may be a transiently evolving process where, initially the BMP is free to diffuse [3], and later becomes tightly localized in the region of previous signaling [5]. We find that when equations (1-8) are solved in the absence of receptor interactions with parameter choices over 4 orders of magnitude, many of the requirements for tight localization of BMP are relaxed and the systems exhibits robustness over a wider range of parameters than those found previously [2]. This is in part due to heterodimer formation (Equations 1-3) of the signaling molecules and part due to downstream dimerization reactions (Sog+Tsg and Sog/Tsg + BMP) (our unpublished data and [1]). For Case 3, the upstream robustness gained by the system at steady-state transfers directly the steady-state distributions of occupied receptors. However, for Case 4 it is less clear how the upstream robustness transfers to the level of occupied receptors yet the distributions of BR still exhibit the observed pMad signaling profiles (Figure 3 main text). What is less clear is how patterning is robust with respect to the level of receptors. It is possible that heterodimer formation of receptor subunits may lead to insensitivity by forming heterodimers [1], but positive feedback of an SBP may also compensate for changes in the level of receptors. In the following section, we compare the sensitivity of Cases 1, 2, and 4 to determine the transient robustness for changes in the level of receptors and other parameter values.

7.2 Sensitivity of receptor interactions.

Do receptor interactions of Cases 1, 2, and 4 transiently hinder or enhance the robustness of patterning? Also, is the width of pMad signaling resilient to both up-regulation of receptors as previously shown [3, 5] and down-regulation of receptors as shown in the zygotic *tkv* mutant (Figure 18). To help answer these questions we determined the number of cells near the dorsal midline whose level of occupied receptors is greater than a specified threshold

value for changes in the parameters and levels of the species involved.

_wt_   _tkv⁻/⁻_
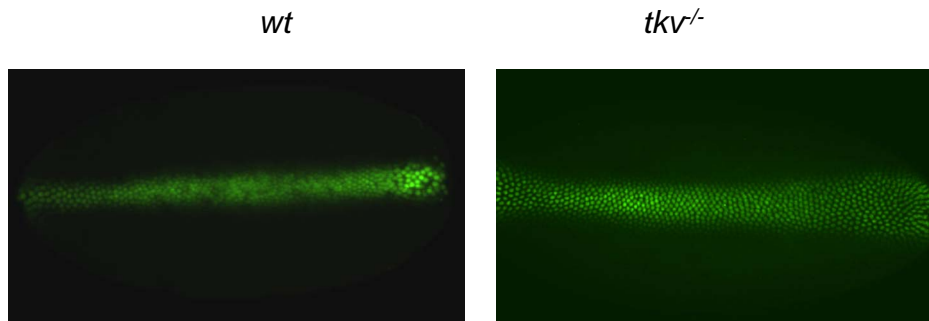
Figure 18: pMad staining in embryos lacking zygotic _tkv_ exhibit _wt_ like signaling profiles. Embryos are homozygous for tkv^7.

Choice of parameter values. First, a base case set of parameters for modules I and II was selected and held constant for the different receptor schemes. The parameters used for this study are given in Table 1. Next, parameters were selected for three different versions of module III: Case 1- equilibrium receptor binding, Case 2- receptor binding with endocytosis, or Case 4- positive feedback with endocytosis. We decided to keep the receptor binding and endocytosis rate parameters fixed for the three cases. Since the range of plausible receptor levels spans 4 orders of magnitude (see section 5), we vary these for each model, with everything else constant, and choose values so the models are in a similar dynamic range. For Case 1 at 60 minutes, the BMP vs. BMP-receptor curve is linear up to a concentration of $\approx 10\mu M$ suggesting the transient effects are negligible and we choose a concentration of receptors of $3.2\mu M$ and an amplitude of $\approx 30nM$ for BMP-Receptor. To determine the level of receptors for Case 2, we chose the level of receptors that corresponds to the maximum amplitude at 60 min since this would have the sharpest extracellular distribution due to rapid receptor mediated endocytosis. This gives a receptor concentration of $3.2\mu M$. The maximum amplitude for Case 4 gives a receptor concentration of 320 nM which is twice the value used in the main text. Transient results for these choices of parameters are provided in Figures 8, 10, and 13. The BMP-Receptor amplitude at the dorsal midline vs. receptor

33

level is shown in Figure 19.
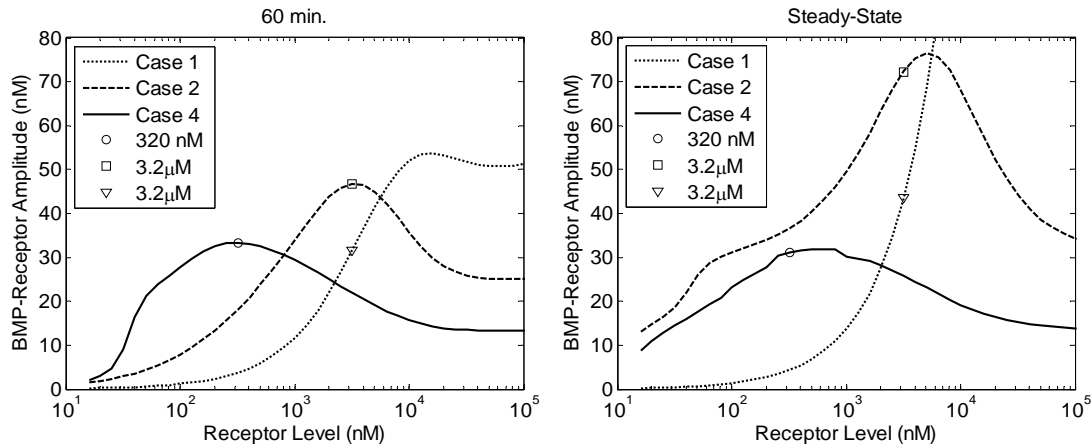
Figure 19: Dorsal midline amplitude dependence on receptor level for different cases of Module III. Also shown is the amplitude for specific choices of parameters for Case 1($\triangledown$), Case 2($\square$), and Case 4($\circ$)

Sensitivity to receptor levels and threshold selection. With the base parameters for Cases 1, 2, and 4 selected, we quantified the response of the system to changing the levels of receptors from the base case. Specifically, receptor levels in the PV space were varied from 16nM ($\approx$120 receptors/cell) up to $1.6 \cdot 10^5$ nM ($\approx$1.2 $\cdot$ 10^6 receptors/cell) which is slightly larger than the range given in section 5. Transient solutions were computed and normalized to the 60 minute amplitude of BR for the base case of each model. Next, a signaling threshold was selected for the base case at 60 min. and cells were sorted as either high or low signaling based on the local BR level. If cells have BR levels above the normalized threshold, they are counted as high signaling cells. The total number of cells with BR above the threshold give the expected width of the region of high pMad signaling along the dorsal surface. In general, Case 1 and 2 are much more sensitive to the specific choice of threshold value than Case 4 in which the distribution is sharp at 60 minutes and forms a spatial discontinuity at steady-state. Results for the sensitivity of each model for changes in the level of receptor for threshold choices between 0.4-0.6 of the base case are shown in Figure 20.
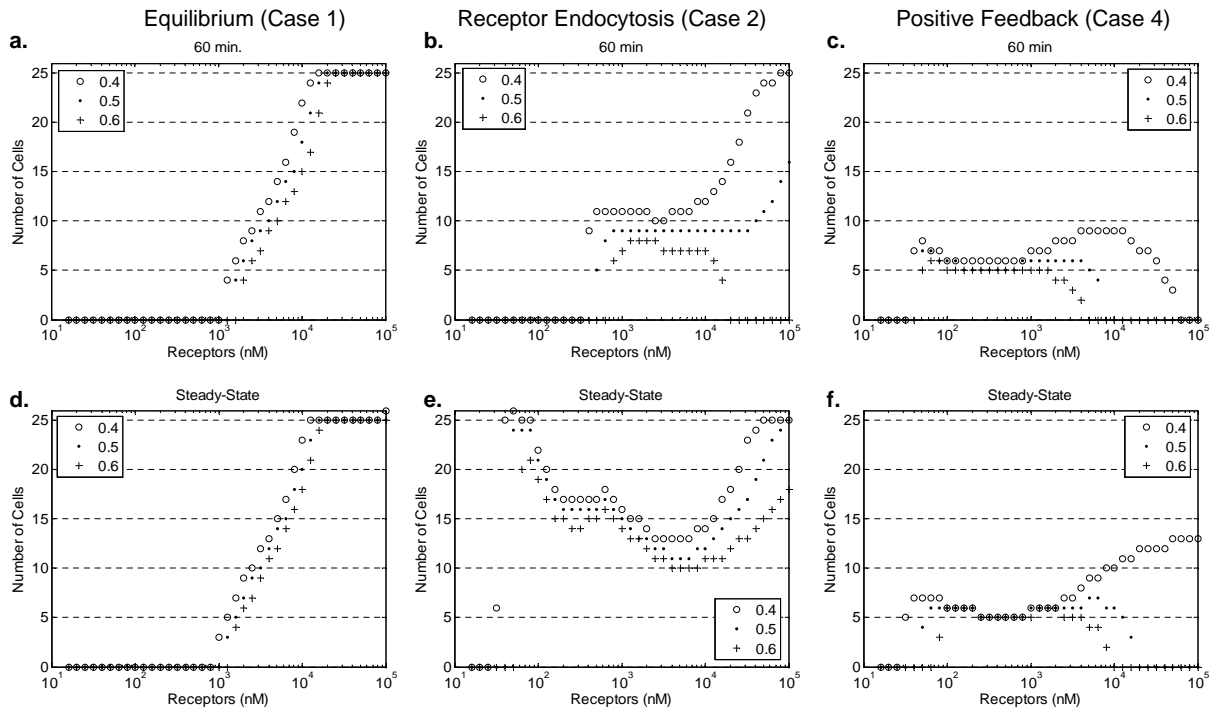
Figure 20: Sensitivity to the receptor levels. Results are shown at 60 min (a-c) and steady-state (d-f) for Case 1 (a,d), Case 2 (b,e) and Case 4 (c,f). The width in number of cells expected to have a high signaling fate according to threshold level selected as a fraction of the base case maximum (0.4 ∘, 0.5 ·, or 0.6 +).

Case 1 exhibits the most sensitivity to changes in receptor level at both 60 minutes and steady state (20a,d). For receptor levels below $\approx 10^3$ nM the maximum amplitude is below the threshold value 0.4 of the base case. For receptor levels above $\approx 10^4$ nM, the width of the high signaling region encompasses the entire dorsal half. The result is not very sensitive to the threshold level and the number of cells changes by $+/-1$ depending on the specific choice. Case 2 exhibits less sensitivity to changes in the level of receptors than 1 at both 60 minutes and steady-state (Figure 20b,e). Case 2 is more sensitive to the specific threshold choice than 1 and a threshold choice of 0.5 is the least sensitive to changes in the level of receptors (20b) at 60 minutes and the number of cells at this threshold choice changes by less than $+/-$ 2 cells for a range of receptors from $\approx 6 \cdot 10^2$ to $4 \cdot 10^4$ nM. At steady-state, however, the results are significantly more sensitive with a range that meet the same criteria of $\approx 1 \cdot 10^3$ to $2 \cdot 10^4$ nM. Case 4 exhibits the least sensitivity to the specific choice of threshold among the three cases at 60 minutes and steady-state (Figure 20c,e). (Note: At steady-state this is principally a property of the spatial bi-stability which leads to a discontinuity in the spatial derivative. However at 60 minutes before the system has completely evolved to bi-stability, the positive feedback contributes to the steepness of the gradient and is not the result of a spatial discontinuity of the derivative.) For a threshold value of 0.5, the acceptable range of receptor level is anywhere between $\approx 5 \cdot 10^1$ and $6 \cdot 10^3$ nM at 60 minutes which expands to $\approx 5 \cdot 10^1$ and $1.2 \cdot 10^4$ nM at steady-state. Considering that the possible range for receptor levels varies between $\approx 3.9 \cdot 10^1$ and $1.6 \cdot 10^4$ nM (Section 5), positive feedback of an SBP may be a component that significantly reduces the sensitivity of morphogen gradient interpretation to the specific level of receptors.

Sensitivity to receptor/SBP kinetic rate parameters. We were interested specifically in the sensitivity of the system to specific choices of the receptor/ligand binding parameters, and for the positive feedback model, the SBP binding parameters. To evaluate the sensitivity we varied the kinetic rates over three orders of magnitude from 10^{-2} to 10^1 nM^{-1}min^{-1} for second order reactions or min^{-1} for first order reactions. As described in the previous paragraph, cells were sorted according to the threshold level of 0.5 of the maximum amplitude

of the base case. The results at 60 minutes and steady-state for variation in the forward and reverse binding rates are shown in Figure 21.
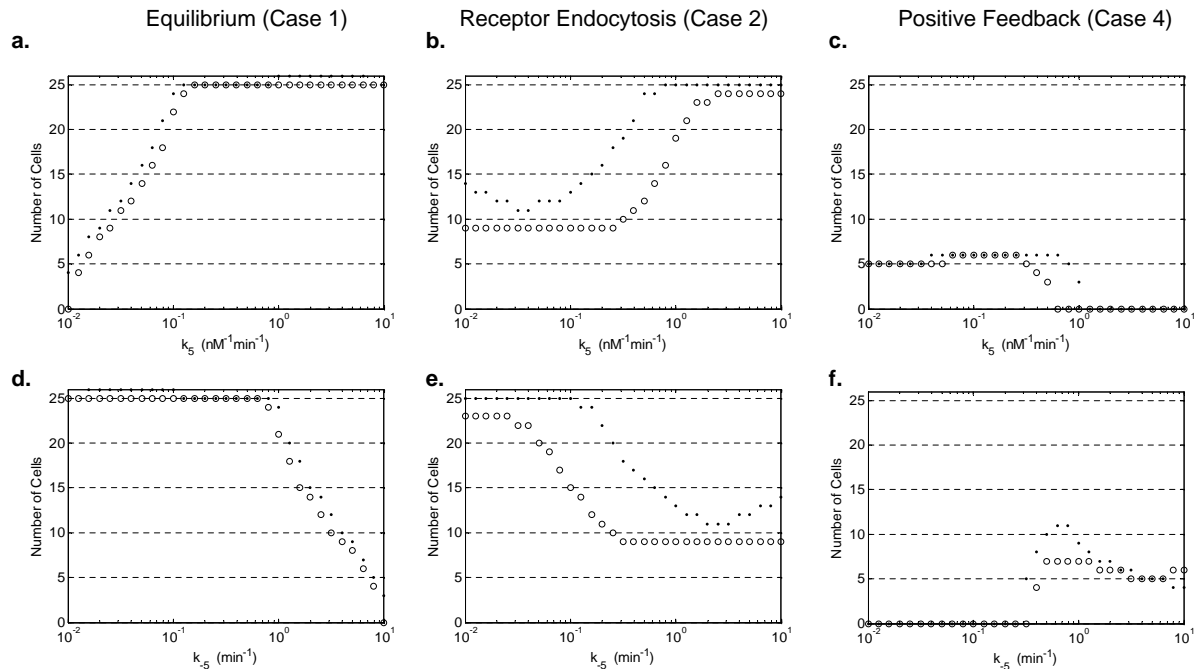
Figure 21: Sensitivity to the receptor binding parameters k_5 (k_{on}) (a-c) and k_{-5} (k_{off}) (d-e). Results are shown at 60 min (∘) and steady-state (·) for Case 1(a,d), 2 (b,e) and 4(c,f).

Here Case 1 is most sensitive to the binding rate whereas Case 2 is less sensitive for receptor binding rates from 10^{-2} to $2 \cdot 10^{-1} nM^{-1} min^{-1}$. Case 4 receptor binding can vary from 10^{-2} to $10^0 nM^{-1} min^{-1}$ at steady-state which is less sensitive than either Case 1 or 2.

Similarly, for Case 4, the sensitivity for SBP kinetic rates are shown in Figure 22.

Case 4 is insensitive to k_4, k_{-4} and k_6 but requires high off-rates k_{-6} and k_{-7}. The width in number of cells for changes in k_7 (the transfer of BMP from receptor to SBP) is fairly insensitive.

Deviations of local dynamics and bi-stability. To address the dependence of the bistable output on the specific choices of parameters, equilibrium solutions were computed for receptor and SBP interactions by varying each of the parameters independently. A
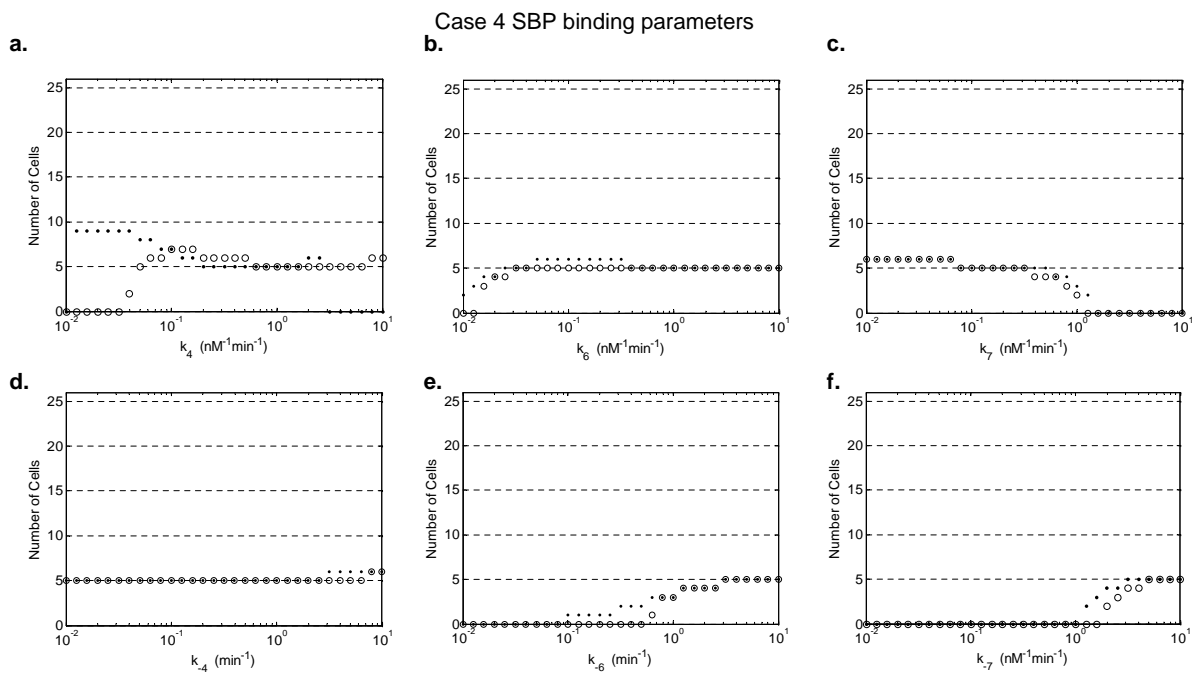
Figure 22: Sensitivity to the SBP binding parameters for Case 4. Results are shown at 60 min (∘) and steady-state (·).

receptor concentration of 160nM was used for this study, however results for 320nM are qualitatively similar. Substituting in the conservation condition on receptors, scaling time by the slow degradation parameter (δ) and concentration by the total number of receptors R_{tot}, and dividing by a large parameter leads to the singularly perturbed version of the receptor interactions. The redistribution of BMP amongst the various cell surface components occurs rapidly relative to the slow positive feedback. We simulated the dimensionless equations using Matcont bifurcation software for Matlab [17]. First, an integrator was used to find a good initial guess. Then, we solved for the equilibrium solution and step backwards in the level of extracellular BMP. The output equilibrium solution for the level of BMP bound receptor vs. the level of extracellular BMP is plotted and S shaped equilibrium curves show the presence of a bistability in the level of BMP.

$$\frac{[B]}{[R_0]} = \beta, \ \frac{[BC]}{[R_{tot}]} = u, \ \frac{[BCR]}{[R_{tot}]} = w, \ \frac{[BR]}{[R_{tot}]} = v, \ \frac{[C_{tot}]}{[R_{tot}]} = \alpha$$

$$\delta = \delta_E + \delta_D, \ \ t = \tau/\delta$$

$$0 = \beta \left(\alpha - u - w \right) - \frac{(k_{-4} + \delta)}{k_4 [R_{tot}]} u - \frac{k_6}{k_4} \left(1 - v - w \right) u + \frac{k_{-6}}{k_4 [R_{tot}]} w \tag{35}$$

$$0 = \frac{k_6}{k_4} \left(1 - v - w \right) u + \frac{k_7}{k_4} \left(\alpha - u - w \right) v - \left(\frac{k_{-6} + k_{-7} + \delta}{k_4 [R_{tot}]} \right) w \tag{36}$$

$$0 = \frac{k_5 \beta}{k_4} \left(1 - v - w \right) - \frac{(k_{-5} + \delta_E)}{k_4 [R_{tot}]} v - \frac{k_7}{k_4} (\alpha - u - w) v + \frac{(k_{-7} + \delta_D)}{k_4 [R_{tot}]} w \tag{37}$$

$$\frac{d\alpha}{d\tau} = \frac{\frac{\Lambda}{\delta [R_{tot}]} v^\nu}{\frac{K_h^\nu}{[R_{tot}]^\nu} + v^\nu} - \alpha \tag{38}$$

Equilibrium solutions for v and β for different choices of parameters are given in Figures 23 and 24. For these computations, δ_E=0 and δ =δ_D=3·10^{-3}min^{-1}. However since δ is a very small parameter, this is equivalent to the case δ_E=3·10^{-3}min^{-1}.

The changes in equilibrium curves of v vs. β for changes in the kinetic parameters do not generally correspond with the sensitivity of the full patterning model for changes in the same parameter. For instance, the full model is not very sensitive to the parameters k_4 and
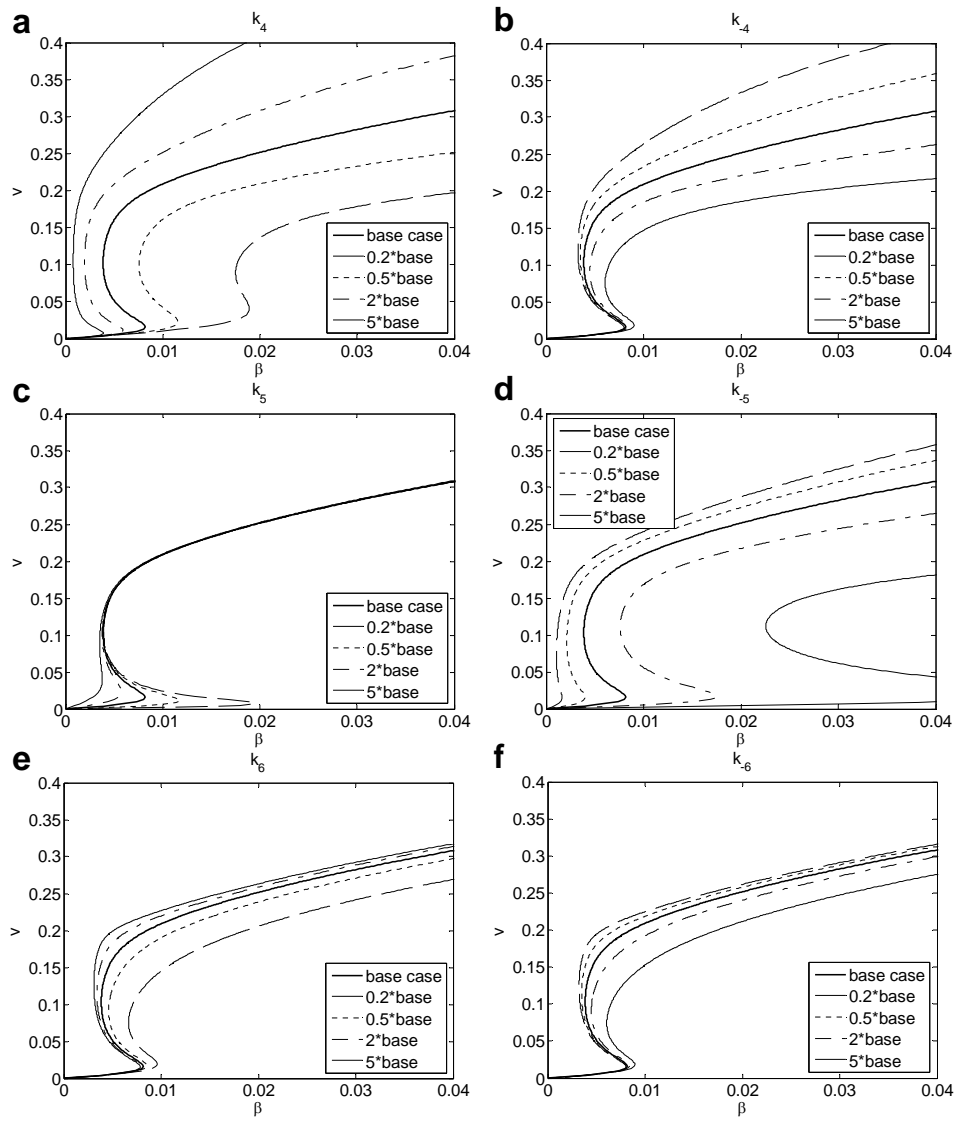
Figure 23: Equilibrium diagrams for positive feedback parameters.
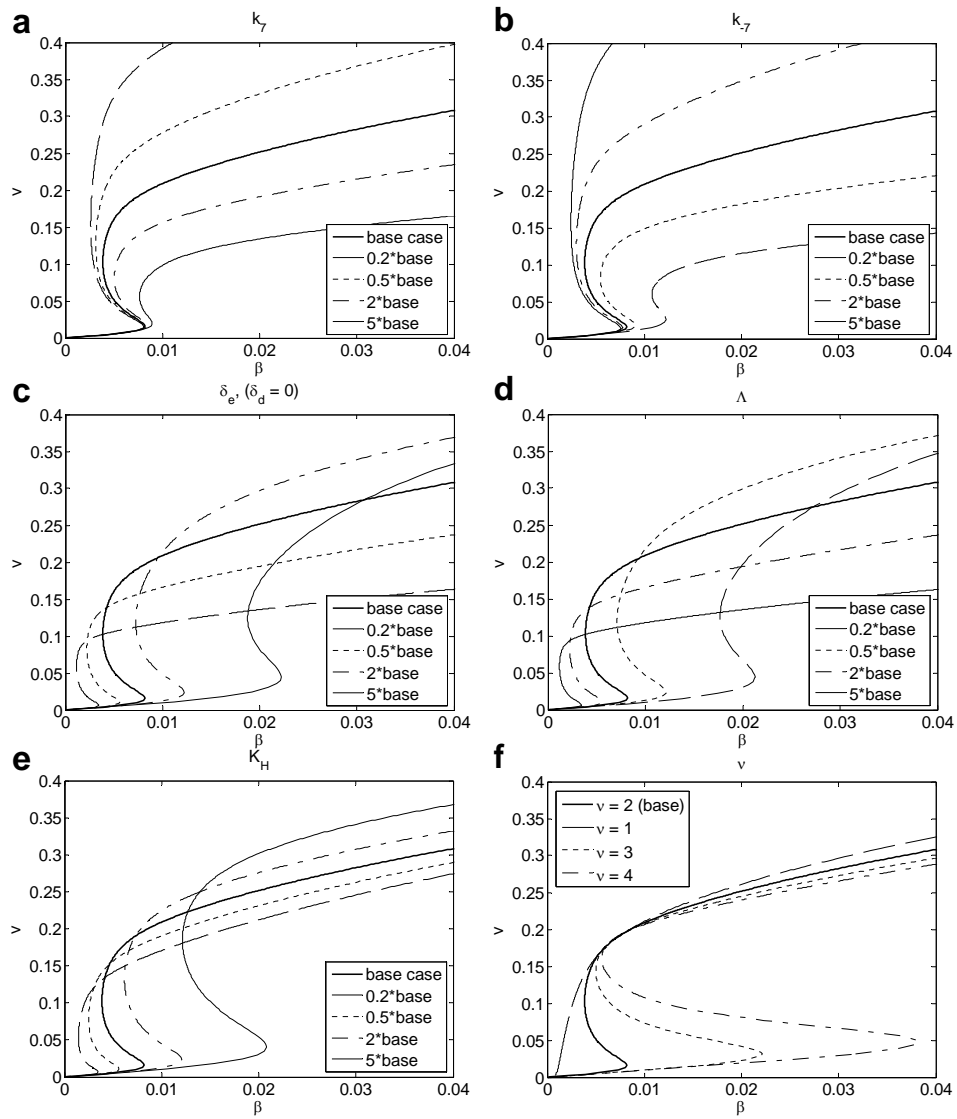
Figure 24: Additional equilibrium diagrams for positive feedback parameters.

k_{-4} as shown in Figure 22, however the local equilibrium curves are much more sensitive to parameter changes in a similar range (Figure 23 a, b). Increases in the parameter k_4 (B on-rate to C) shifts the position of the limit points to the left and increases the level of v for any given level of β. Interestingly, increases in the parameter k_5 (B on-rate to R) also shifts the position of the lower limit point to the left while the upper limit point is stationary and the level of v on the upper stable branch is essentially constant (Figure 23 c). The equilibrium is not very sensitive to changes in k_{-4}, however it is highly sensitive to k_{-5} (Figure 23 b,d). The equilibrium is not very sensitive to changes in k_6 or k_{-6} (BC to R on- and off-rates). The level of v is highly sensitive to changes in k_7 and k_{-7} (BR to C on- and off-rates)(Figure 24 a,b). Of the remaining parameters for the local dynamics: degradation (δ_E), SBP production (Λ), half maximal concentration (K_H), and Hill coefficient (ν), the least sensitive parameter is ν which shifts the lower limit point to the right as the parameter is increased (Figure 24 c-f).

7.3   Sensitivity to parameters of Module I and II

We computed the sensitivity of patterning to the extracellular binding parameters for inhibitor formation, and inhibitor binding to BMP. We did not address the sensitivity with respect to changes in the hetero/homodimer formation rates which are were looked at previously [1].

Sensitivity to extracellular kinetic rate parameters   First, we looked at the sensitivity to Sog + Tsg binding. Figure 25 demonstrates that all the different cases of Module III are insensitive to the reverse step k_{-2}, however cases 1and 2 exhibit a similar sensitivity to k_2 with a wide distribution that narrows as the forward binding rate increases. Case 4 is very insensitive at 60 minutes, however for values of k_2 below 10^{-1} nM^{-1}min^{-1}, peak splitting occurs and no centralized BMP peak forms.

For the binding of the Sog/Tsg complex (I) to BMP, all versions of Module III are virtually insensitive to the off-rate k_{-3} (Figure 26 d,e,f). For the on-rate k_3, Cases 1 and 2 exhibit similar behavior where slow binding leads to very wide distributions at steady-state
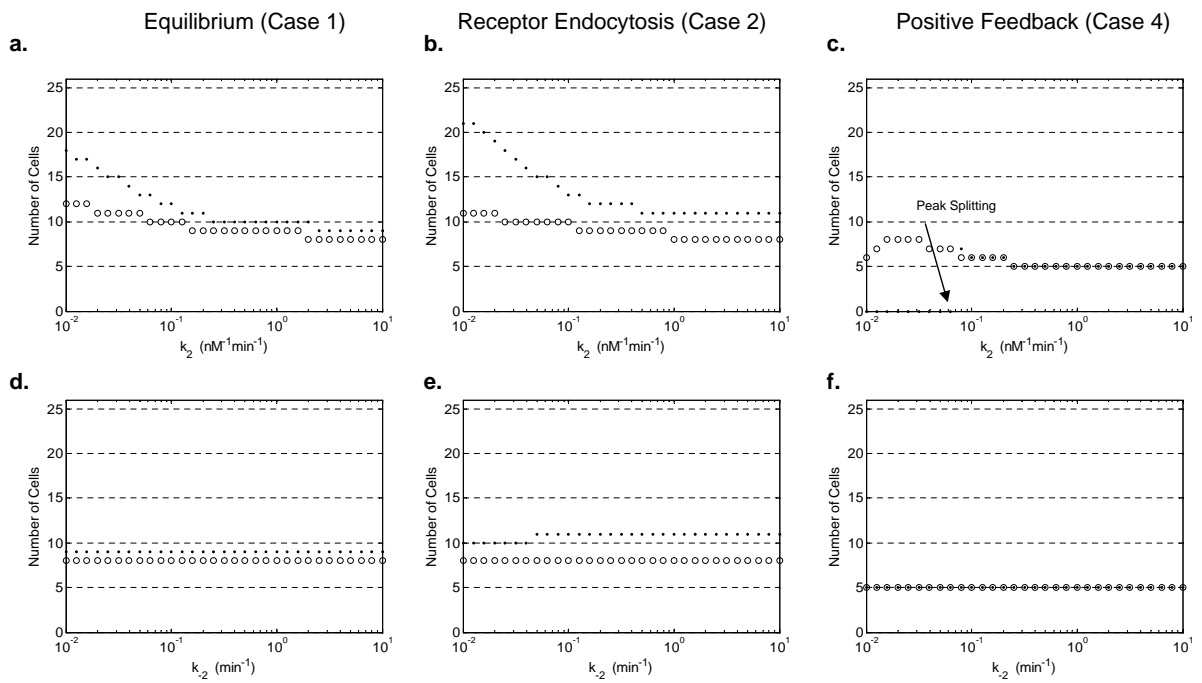
Figure 25: Sensitivity to Sog and Tsg binding parameters k_2 (k_{on}) (a-c) and k_{-2} (k_{off}) (d-e). Results are shown at 60 min ($\circ$) and steady-state ($\cdot$) for Case 1 (a,d), 2 (b,e) and 4 (c,f).

that narrow as binding increases. For Case 4, appropriate distributions at 60 minutes are achieved with with k_3 values greater than $6 \cdot 10^{-1}\text{nM}^{-1}\text{min}^{-1}$. However, for long times, peak splitting can occur due to inefficient transport and normal patterning at steady-state requires that $k_3 \approx 2\text{nM}^{-1}\text{min}^{-1}$ or higher.
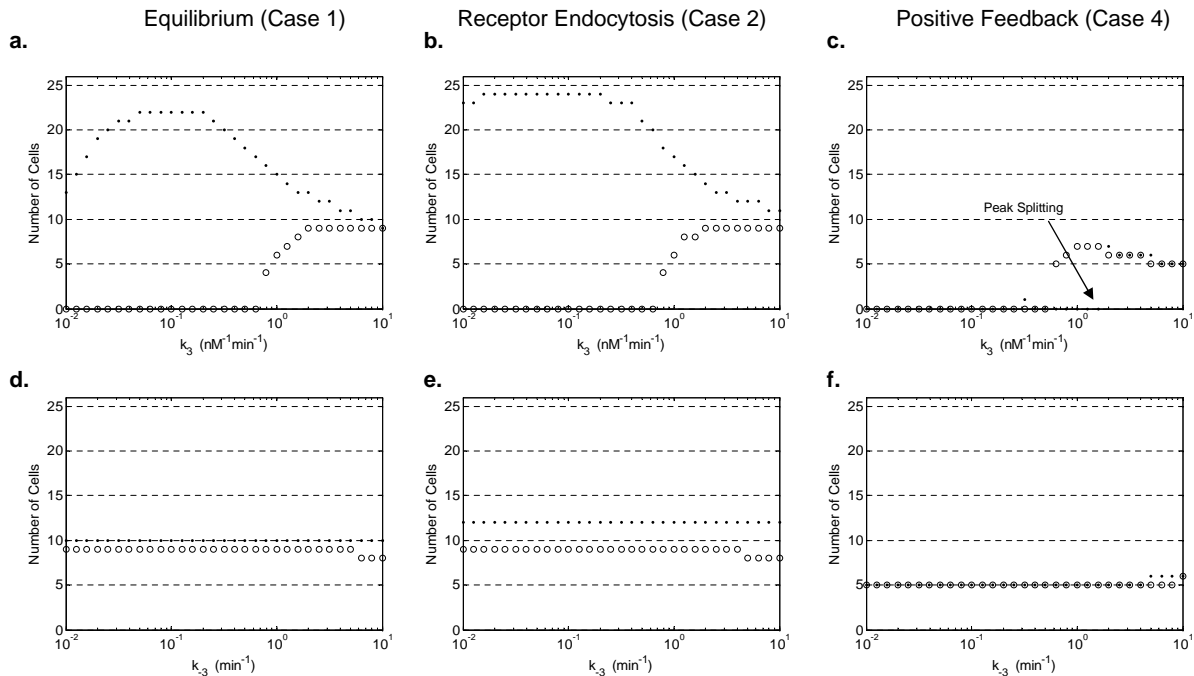
Figure 26: Sensitivity to Sog/Tsg binding to Dpp/Scw k_3 (k_{on}) (a-c) and k_{-3} (k_{off}) (d-e). Results are shown at 60 min (○) and steady-state (·) for Case 1 (a,d), 2 (b,e) and 4 (c,f).

Sensitivity to embryo size   With a decent estimate for the diffusion coefficients [11] we did not calculate the sensitivity of patterning to the specific value of each diffusion coefficient. Instead, we calculated the sensitivity of patterning to the size of the embryo by scaling all the diffusion coefficients simultaneously. The size of the embryo was varied from 0.25 of *wt* up to 1.75 X *wt* and the width of presumptive amnioserosa in number of cells was computed as before.

Case 1 and 2 behave similarly and produce patterns that are wide for small embryos but are largely insensitive for larger embryos. Case 4 scales well for small embryos but for
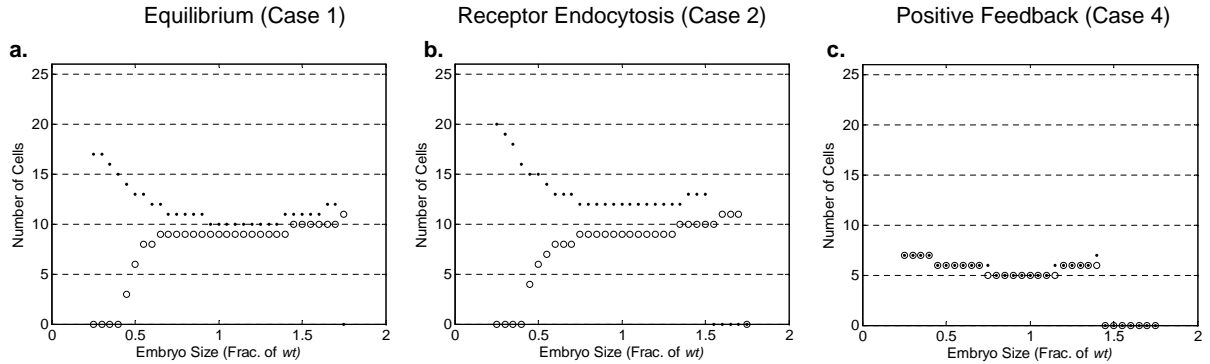
Figure 27: Sensitivity to embryo size for different versions of module III as a fraction of the *wt* embryo cross-section. Results are shown at 60 min (○) and steady-state (·) for Case 1 (a), 2 (b) and 4 (c).

embryos 1.5 X and larger, the removal is too rapid for Sog mediated redistribution of BMP.

7.4   Abnormal model behavior: peak splitting

For long times, some parameters gave rise to peak splitting during the sensitivity analysis. Instead of forming a peak centered near the dorsal midline, these profiles exhibit multiple maxima throughout the dorsal region. An example of this occurs in *sog* homozygous mutant embryos where, if patterning persists long enough the positive feedback causes the shallow dorsal peak to split and as time progresses the profile forms additional peaks. Profiles that exhibited this type of behavior during the sensitivity analysis were penalized by setting the number of cells above a threshold as zero and identified on the corresponding figures.
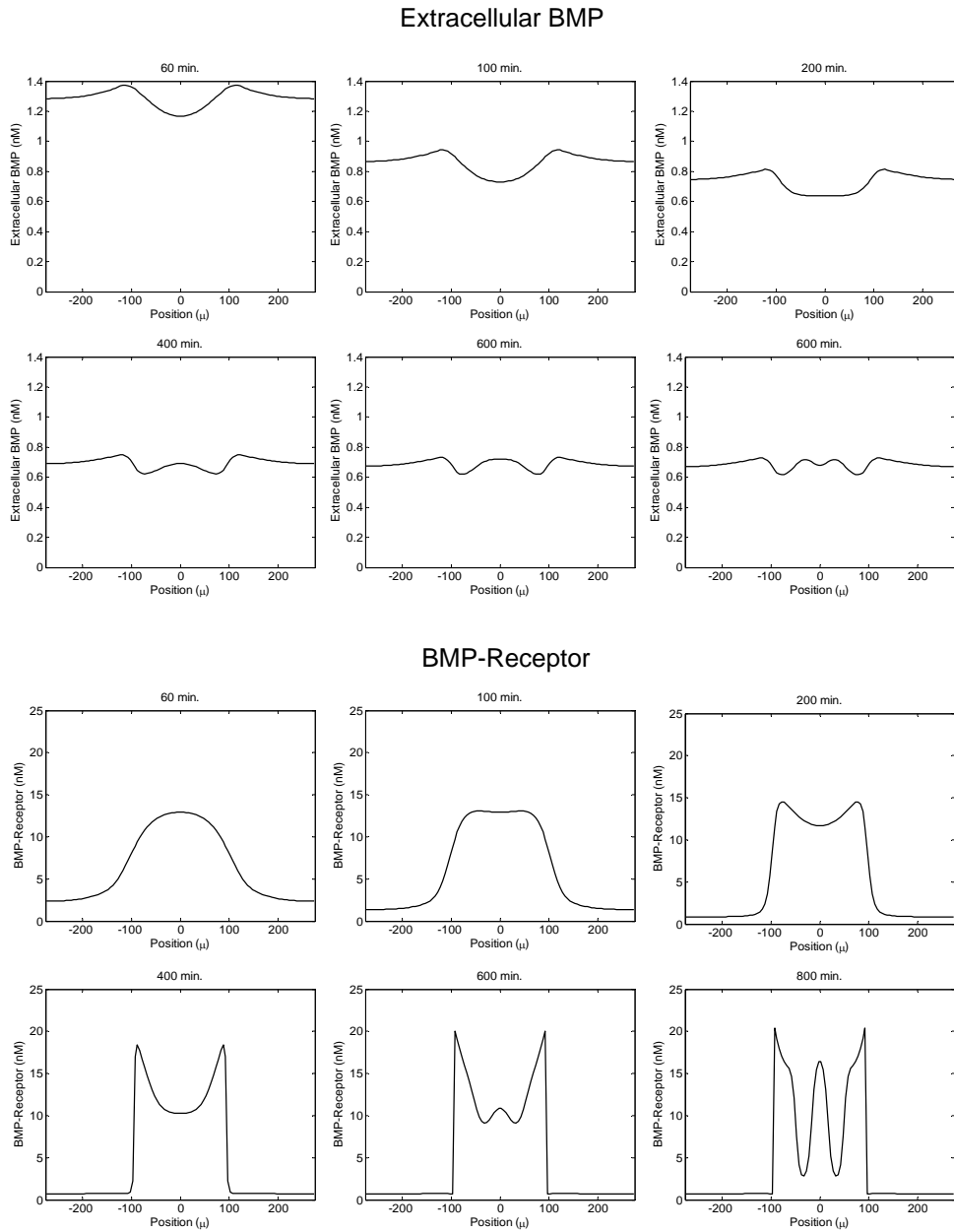
Figure 28: During the numerical screen, positive feedback can lead to a peak splitting behavior where the peak at the dorsal midline begins to split when the removal rate becomes greater than the rate at which additional BMP is supplied to the limiting area. A typical evolution depicting peak splitting behavior is shown here.

46

References

[1] O. Shimmi, D. Umulis, H. Othmer, and M. Connor. Faciliated transport of a Dpp/Scw heterodimer by Sog/Tsg leads to robust patterning of the Drosophila blastoderm embryo. *Cell*, 120(6):873–886, 2005.

[2] A. Eldar, R. Dorfman, D. Weiss, H. Ashe, B. Z. Shilo, and N. Barkai. Robustness of the BMP morphogen gradient in *Drosophila* embryonic patterning. *Nature*, 419(6904):304–8, 2002.

[3] C. M. Mizutani, Q. Nie, F. Y. Wan, Y. T. Zhang, P. Vilmos, R. Sousa-Neves, E. Bier, J. L. Marsh, and A. D. Lander. Formation of the BMP activity gradient in the Drosophila embryo. *Dev. Cell*, 2005.

[4] M. B. O'Connor, D. Umulis, H. G. Othmer, and S. S. Blair. Shaping bmp morphogen gradients in the drosophila embryo and pupal wing. *Development*, 133(2):183–93, 2006.

[5] Y. C. Wang and E. L. Ferguson. Spatial bistability of Dpp-receptor interactions during Drosophila dorsal-ventral patterning. *Nature*, 434:229–34, 2005.

[6] H. Mitchell, A. Choudhury, R. E. Pagano, and E. B. Leof. Ligand-dependent and -independent transforming growth factor-beta receptor recycling regulated by clathrin-mediated endocytosis and Rab11. *Mol Biol Cell*, 15(9):4166–78, 2004.

[7] D. A. Lauffenburger and J. J. Linderman. *Receptors: Models for binding, trafficking and signaling.* Oxford University Press, Oxford, New York, 1993.

[8] S. Dyson and J. B. Gurdon. The interpretation of position in a morphogen gradient as revealed by occupancy of activin receptors. *Cell*, 93(4):557–568, 1998.

[9] A. R. Tzafriri, D. Wu, and E. R. Edelman. Analysis of compartmental models of ligand-induced endocytosis. *J Theor Biol*, 229(1):127–38, 2004.

[10] O. Shimmi and M. B. O'Connor. Physical properties of Tld, Sog, Tsg and Dpp protein interactions are predicted to help create a sharp boundary in Bmp signals during

dorsoventral patterning of the Drosophila embryo. *Development*, 130(19):4673–4682, 2003.

[11] M. E. Young, P. A. Carroad, and R. L. Bell. Estimation of diffusion coefficeints of proteins. *Biotechnol. Bioeng.*, 22:947–955, 1980.

[12] A. D. Lander, Q. Nie, and F. Y. Wan. Do morphogen gradients arise by diffusion? *Dev Cell*, 2(6):785–96, 2002.

[13] J. Greenwald, J. Groppe, P. Gray P, E. Wiater, W. Kwiatkowski, W. Vale, and S. Choe. The BMP7/Actrii extracellular domain complex provides new insights into the cooperative nature of receptor assembly. *Mol Cell*, 11(3):605–17, 2003.

[14] W. Sebald, J. Nickel, J. L. Zhang, and T. D. Mueller. Molecular recognition in bone morphogenetic protein (BMP)/receptor interaction. *Biol Chem*, 385(8):697–710, 2004.

[15] J. M. Vilar, R. Jansen, and C. Sander. Signal processing in the tgf-beta superfamily ligand-receptor network. *PLoS Comput Biol*, 2(1):0036–45, jan 2006.

[16] F. Rentzsch, J. Zhang, C. Kramer, W. Sebald, and M. Hammerschmidt. Crossveinless 2 is an essential positive feedback regulator of Bmp signaling during zebrafish gastrulation. *Development*, 2006.

[17] A. Dhooge, W. Govaerts, and Yu. A. Kuznetsov. MATCONT: A MATLAB package for numerical bifurcation analysis of ODEs. *ACM Trans. Math. Soft.*, 29(2):141 – 164, 2003.